Model Reduction and Dynamic Aggregation of Grid-forming Inverter Networks

Olaoluwapo Ajala, *Member, IEEE,* Nathan Baeckeland, *Student Member, IEEE,* Brian Johnson, *Member, IEEE,* Sairaj Dhople, *Senior Member, IEEE,* and Alejandro Domínguez-García, *Fellow, IEEE*

***Abstract*—This paper presents a model-order reduction and dynamic aggregation strategy for grid-forming inverter-based power networks. The reduced-order models preserve the network current dynamics as well as the action of the inverter current-reference limiter. Inverters based on droop, virtual synchronous machine, and dispatchable virtual oscillator control are considered, a generic model for all three control strategies is presented, and a smooth function approximation is utilized to represent the action of the current-reference limiter. The network is assumed to be composed of lines with homogeneous l/r ratios. Given such a system, our approach involves three steps. First, time-domain Kron reduction is used to reduce the dimensions of the electrical network model. Next, dynamic aggregate models are developed for parallel-connected inverters. Finally, singular perturbation analysis is used to systematically eliminate fast-varying dynamics in both the network model and the grid-forming inverter single/aggregate models. Numerical simulation results benchmark the response of the reduced-order aggregate models against the full-order models from which they are derived, and we demonstrate significant savings in computation cost with limited loss of accuracy.**

***Index Terms*—Grid-forming control, Current limitation, Droop control, Virtual synchronous machine, Dispatchable virtual oscillator control, Reduced-order modeling, Dynamic aggregation, Singular perturbation analysis.**

I. Introduction

As the displacement of synchronous machines by inverter-based power generation gains momentum, several inverter control strategies that could potentially accelerate this transition have been proposed. Among them, grid-forming (GFM) inverter technologies have received significant attention [1]. GFM inverter-based resources (IBRs) essentially behave as a signal-controlled AC voltage source behind an impedance [2], and their underlying controls may be based on droop [3], [4], virtual synchronous machine (VSM) [5]–[7], virtual oscillator control (VOC) [8], [9], or dispatchable virtual oscillator control (dVOC) [10]–[12].

The dynamic characteristics of GFM IBRs are influenced by several subsystems including, but not limited to, controllers, filters, reference-frame transformations, and current limiters. As a result, electromagnetic transient models for networked GFM IBRs have numerous dynamical states spanning several timescales. To tame model complexity and preserve model accuracy, this paper outlines a comprehensive approach to model reduction and aggregation for networks with GFM IBRs:

- *Model reduction.* This is pursued at the network level and then at a system level. A combination of time-domain Kron reduction and singular perturbation is leveraged to reduce the model-order for the network of GFM inverters, while preserving the network current dynamics and the effects of current limiters.
- *Dynamic aggregation.* A systematic procedure is outlined for scaling parameters of parallel-connected GFM inverters and obtaining an aggregate model that retains the structure of individual GFM inverter models while faithfully capturing the aggregation of all individual resource dynamics in the time domain.[1]

Contributions: The proposed approach yields lower-order models for electrical power networks and GFM IBRs, as well as structure-preserving aggregate models for parallel-connected GFM IBRs of the same type. While model-order reduction and dynamic aggregation for IBRs has received significant attention in the literature (we review prior art shortly), our approach offers notable contributions from three angles:

1) it applies, in a generalized manner, to a variety of GFM IBR control methods (i.e., droop, VSM, dVOC) that are garnering significant attention in the literature;
2) it preserves the impact of current-reference limiting and network current dynamics in the reduced-order models;
3) it leverages dynamic aggregate models that mirror the structure of originating models without any loss in modeling accuracy.

Note that: 1) ensures the universal applicability of the proposed approach in modeling future grids with GFM IBRs of different types. Furthermore, the impact of current-reference limiters

O Ajala and A. Domínguez-García are with the Department of Electrical and Computer Engineering, University of Illinois at Urbana-Champaign, Urbana, IL 61801 USA. E-mail:{ooajala2, aledan}@ILLINOIS.EDU.

N. Baeckeland is with the Department of ESAT, KULeuven, Belgium nathan.baeckeland@kuleuven.be.

S. Dhople is with the Department of Electrical and Computer Engineering, University of Minnesota, Minneapolis, MN 55455 USA. Email: sdhople@UMN.EDU.

B. Johnson is with the Department of Electrical and Computer Engineering, University of Texas, at Austin, TX 78712 USA Email: b.johnson@UTEXAS.EDU

This material is based upon work supported by the U.S. Department of Energy's Office of Energy Efficiency and Renewable Energy (EERE) under Solar Energy Technologies Office (SETO), through the award numbers EE0009025 and 38637 (UNIFI consortium), respectively; and by the Belgian American Educational Foundation. The views expressed herein do not necessarily represent the views of the U.S. Department of Energy or the United States Government.

[1]The terminology of *Dynamic Aggregation* is adopted from classical efforts in the literature on synchronous generators. Over the years, other terms have been put forward to capture the same concept, for instance, *Dynamic Equivalence* finds frequent mention as well.

and network dynamics have been recognized to be relevant in control design and operation of GFM IBRs [13]; this underscores the importance of 2). Finally, with regard to 3), structure-preserving aggregations prevent duplication of dynamic models (i.e., one does not have to develop models for all the GFM inverters in a parallel-connected set) and provide further model-order reductions (i.e., a collection of n dynamical systems can be represented by an equivalent dynamical system) without loss of accuracy. Taken together, the contributions 1)-3) fill gaps in available methods for model reduction from the device and network levels, while capturing salient features of GFM technology (such as the variety in primary control methods and current limiting). The setting also acknowledges the fact that IBRs are routinely connected in parallel to scale capacity in plants (further adding to modeling complexity). Uniquely, all the reduced-order models we put forth (at the device and network level) preserve structure of the originating models. This is a deliberate attempt to ensure the approach is accessible to a wide range of potential users and can be readily implemented in common simulation tools. In general, straight-up application of numerical methods for model reduction do not come with any guarantees on the structure of the reduced-order models.

Literature Review: The development of reduced-order models from full-order models of electric power networks has received significant attention in the literature. Reduced-order models have been developed using coherency and aggregation [14], selective modal analysis [15], synchronic modal equivalencing [16], Kron reduction [17], and singular perturbation analysis [18]. In [19], authors present the model-order reduction of an islanded microgrid using singular perturbation analysis. However, the electrical network dynamics are not considered, and the originating full-order model is not presented. Authors in [20] present a reduced-order Kuramoto-type model for grid-forming inverters that was developed using singular perturbation analysis and Kron reduction; a lossless electrical network is considered and sufficient conditions for which the Kuramoto-type model is valid are presented. In [21], a full-order model for inverter-based microgrids is presented, and singular perturbation analysis is used to perform model-order reduction, as done in this work. However, the small parameters used for singular perturbation analysis are not explicitly identified, details of the model reduction process are not presented, and the impacts of current limiters are not considered. Singular perturbation has been leveraged in several other prior efforts for model reduction of inverter based networks [22]–[27]. However, these approaches do not encompass as comprehensive of a setting as ours, i.e., acknowledging different primary control types, time-domain network dynamics, and dynamic aggregation. In [28] time-domain Kron reduction is used to develop reduced-order models for electrical networks with homogeneous resistance-to-reactance ratios. However, there does not appear to be work that has leveraged time-domain Kron reduction deliberately as part of model reduction in complex networks. Our current effort takes a step in this direction. Note however, that since we build off [28], our approach is constrained to networks that have homogeneous lines.

Notation: The $n \times n$ diagonal matrix with diagonal entries $x_1, \ldots, x_n$ is denoted by $\mathrm{diag}(x_1, \ldots, x_n)$. The identity matrix is denoted by $\mathbb{I}$, the standard-basis column vector with 1 in the k-th position is denoted by $\mathbb{e}_k$, and the all-zeros and all-ones column vectors are denoted by $\mathbb{0}$ and $\mathbb{1}$, respectively. (Dimensions of $\mathbb{I}$, $\mathbb{e}_k$, $\mathbb{0}$, and $\mathbb{1}$ are not specified in the notation but can inferred from context when utilized.)

Reference-frame Transformations: We consider two direct-quadrature rotating reference frames as follows: (i) the DQ reference frame (also referred to as synchronously rotating reference frame), which rotates in synchrony with the system nominal angular frequency—assumed to be constant; and (ii) the dq reference frame, which rotates at a time-varying frequency whose value is determined by the reference angular frequency of a particular GFM inverter (see [29, pp. 69–114] for more details). In the remainder, all three-phase variables and companion signals are represented in either the DQ or dq reference frames. Corresponding to three-phase signal

$$f(t) = [f_a(t),\, f_b(t),\, f_c(t)]^\top,$$

we write $f'(t) = [f_D(t),\, f_Q(t)]^\top$ and $f''(t) = [f_d(t),\, f_q(t)]^\top$ to denote its DQ and dq representation, respectively. Define

$$\delta(t) = \delta_0 + \int_0^t (\omega^\circ(x) - \omega_0)\, dx, \tag{1}$$

with $\delta_0 = \delta(0)$, and where ω_0 and $\omega^\circ(t)$ respectively denote the nominal angular frequency and the reference angular frequency of a particular GFM inverter. Then, $f(t)$, $f'(t)$ and $f''(t)$ are related via

$$f'(t) = \overline{\mathrm{T}}(\omega_0 t) f(t), \tag{2a}$$

$$f''(t) = \mathrm{T}(\delta(t)) f'(t), \tag{2b}$$

where $\mathrm{T}(\cdot)$, and $\overline{\mathrm{T}}(\cdot)$ are transformation matrices given by

$$\overline{\mathrm{T}}(\theta) = \frac{2}{3}\begin{bmatrix} \cos\theta & \cos(\theta - \frac{2\pi}{3}) & \cos(\theta + \frac{2\pi}{3}) \\ -\sin\theta & -\sin(\theta - \frac{2\pi}{3}) & -\sin(\theta + \frac{2\pi}{3}) \end{bmatrix},$$

$$\mathrm{T}(\theta) = \begin{bmatrix} \cos\theta & \sin\theta \\ -\sin\theta & \cos\theta \end{bmatrix}.$$

Henceforth, we will simplify the adopted notation by dropping the time argument in all quantities.

Paper Organization: In Section II, full-order models for droop-, VSM-, and dVOC-based GFM inverters are overviewed, whereas the full-order model for electrical power networks is presented in Section III. Reduced-order models for GFM inverters and electrical power networks are presented in Section IV. Numerical results that compare the response of the reduced-order models with those of the full-order models are presented in Section V. Concluding remarks are given in Section VI.

II. The Grid-forming Inverter Model

In this section, we present averaged full-order dynamical models for the GFM inverter; these are developed in detail and validated in, e.g., [3], [6], [26], [29]. They include mathematical models for a current-reference limiter, an LCL filter, two proportional-integral (PI) controllers, and a primary controller.

This article has been accepted for publication in IEEE Transactions on Power Systems. This is the author's version which has not been fully edited and content may change prior to final publication. Citation information: DOI 10.1109/TPWRS.2022.3229970

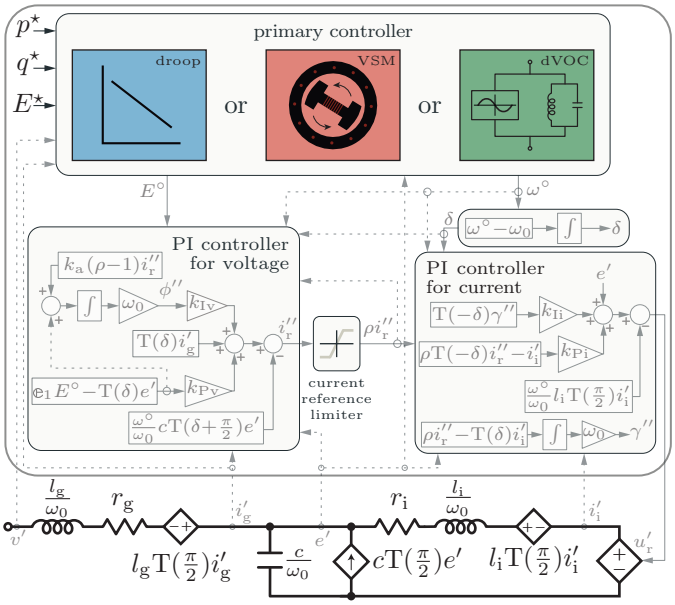

Fig. 1: Schematic diagram of the averaged full-order GFM-inverter model. Inverter control variables and LCL filter variables are represented in the dq and DQ reference frames, respectively.

The current-reference limiter serves to prevent over-current conditions, the LCL filter suppresses switching-frequency ripple at the output, and the proportional-integral (PI) controllers regulate the inverter output current and voltage across the filter capacitor. The primary controller governs the response of the inverter voltage magnitude and frequency references to deviations in output power (measured at the capacitive terminals of the LCL filter, in our implementation). In this paper, we consider droop, VSM, and dVOC primary controls (see [30] for detailed descriptions of each of these).

A schematic representation of the models, in dq and DQ frames, is depicted in Fig. 1. The GFM inverter model is presented in per-unit form (see, e.g., [31, p. 75] for details), and the inverter rated three-phase power, rated line-to-line voltage (RMS), and nominal frequency, denoted by s_b [VA], e_b [V], and ω_0 [$\mathrm{rad\,s^{-1}}$], respectively, are utilized as base quantities. Table I summarizes the normalized parameters, their units, and their respective base values.[2]

A. The Current Limiter, PI Controllers, and LCL filter

Let i'_i and i'_g denote the inverter- and grid-side currents of the filter, respectively, and let e' and v' respectively denote the capacitor voltage and the voltage of the bus at which the GFM inverter is connected. The voltage magnitude and frequency references for the GFM inverter are denoted by E° and ω°, respectively, state variables of the PI controllers that regulate voltage and current are denoted by ϕ'' and γ'', respectively,

[2]The inertia constant is normalized to $\mathrm{s^2\,rad^{-1}}$, not to per unit. This is consistent with the units of the inertia coefficient $\frac{2H}{\omega_0}$ that is used in per-unit synchronous-machine models. (See, e.g., the inertia constant defined in [31, pp. 128–136].) In a similar fashion, the frequency-droop coefficient and the damping coefficient are both normalized to $\mathrm{s\,rad^{-1}}$, not to per unit.

TABLE I: Normalized model parameters for droop-, VSM-, and dVOC-based GFM inverters.

Symbol	Description	Unit	Base value	Actual unit
ω_0	nominal frequency	$\mathrm{rad\,s^{-1}}$		
ω_c	cut-off frequency	$\mathrm{rad\,s^{-1}}$	N/A	N/A
ψ	rotation angle parameter	rad		
i_max	peak current limit	pu	$\frac{s_\mathrm{b}\sqrt{2}}{e_\mathrm{b}\sqrt{3}}$	A
l_i	inverter-side inductance	pu	$\frac{e_\mathrm{b}^2}{s_\mathrm{b}\omega_0}$	H
l_g	grid-side inductance	pu		
c	filter capacitance	pu	$\frac{s_\mathrm{b}}{e_\mathrm{b}^2\omega_0}$	F
r_i	inverter-side resistance	pu		
r_g	grid-side resistance	pu	$\frac{e_\mathrm{b}^2}{s_\mathrm{b}}$	Ω
k_a	anti-windup gain	pu		
k_Pi	proportional gain (current control)	pu		
k_Ii	integral gain (current control)	pu	$\frac{e_\mathrm{b}^2\omega_0}{s_\mathrm{b}}$	$\mathrm{F^{-1}}$
κ_1	synchronization gain	pu		
k_Pv	proportional gain (voltage control)	pu	$\frac{s_\mathrm{b}}{e_\mathrm{b}^2}$	Ω^{-1}
k_Iv	integral gain (voltage control)	pu	$\frac{s_\mathrm{b}\omega_0}{e_\mathrm{b}^2}$	$\mathrm{H^{-1}}$
κ_2	voltage-magnitude control gain	pu	$\frac{3\omega_0}{2e_\mathrm{b}^2}$	$\mathrm{rad\,s^{-1}\,V^{-2}}$
m_f	inertia constant	$\mathrm{s^2\,rad^{-1}}$	$\frac{s_\mathrm{b}}{\omega_0}$	$\mathrm{F\,s\,V^2}$
d_f	frequency droop coefficient	$\mathrm{s\,rad^{-1}}$	s_b	$\mathrm{F\,V^2}$
d_d	damping coefficient	$\mathrm{s\,rad^{-1}}$		
d_v	voltage droop coefficient	pu	$\frac{s_\mathrm{b}}{e_\mathrm{b}\omega_0}$	$\mathrm{F\,V}$
$k_{\mathrm{P}\theta}$	proportional gain (PLL)	pu	$\frac{\omega_0}{e_\mathrm{b}}$	$\mathrm{rad\,s^{-1}\,V^{-1}}$
$k_{\mathrm{I}\theta}$	integral gain (PLL)	pu	$\frac{\omega_0^2}{e_\mathrm{b}}$	$\mathrm{rad^2\,s^{-2}\,V^{-1}}$

and the corresponding controller outputs are denoted by i''_r and u'_r, respectively.

1) Current Limiter: As shown in Fig. 1, the current-reference limiter acts on the output of the voltage controller, i''_r, and generates a revised (limited) reference for the current controller, denoted by $\widetilde{i''_\mathrm{r}}$, as follows:

$$\widetilde{i''_\mathrm{r}} = \min\left(1, \frac{i_\mathrm{max}}{\|i''_\mathrm{r}\|_2}\right) i''_\mathrm{r}, \tag{3}$$

where i_max denotes the maximum permitted value of $\|i''_\mathrm{r}\|_2$ [13]. To ensure that equations constituting the grid-

forming inverter model are continuously differentiable functions of their arguments (as described in [32, p. 2], this is a regularity condition for model-order reduction via singular perturbation analysis), in this paper, we employ the following smooth approximation of (3):

$$\widetilde{i''_{\mathrm{r}}} = \rho i''_{\mathrm{r}}, \tag{4a}$$

where

$$\rho = -\varepsilon \ln\left(\exp\left(-\frac{1}{\varepsilon}\right) + \exp\left(-\frac{i_{\max}}{\varepsilon \|i''_{\mathrm{r}}\|_2}\right)\right); \tag{4b}$$

one can check that $\rho \to \min\left(1, \frac{i_{\max}}{\|i''_{\mathrm{r}}\|_2}\right)$ as $\varepsilon \to 0$ (see [12] for details).

2) PI Controllers: Given (4), the dynamics of the PI controllers can be described by

$$\frac{\mathrm{d}\phi''}{\mathrm{d}t} = \omega_0(\mathbb{e}_1 E^\circ - \mathrm{T}(\delta)e') + \omega_0 k_{\mathrm{a}}(\rho - 1)i''_{\mathrm{r}}, \tag{5a}$$

$$i''_{\mathrm{r}} = k_{\mathrm{Pv}}(\mathbb{e}_1 E^\circ - \mathrm{T}(\delta)e') + k_{\mathrm{Iv}}\phi'' + \mathrm{T}(\delta)i'_{\mathrm{g}} - \frac{\omega^\circ}{\omega_0} c\mathrm{T}(\delta + \tfrac{\pi}{2})e', \tag{5b}$$

$$\frac{\mathrm{d}\gamma''}{\mathrm{d}t} = \omega_0(\rho i''_{\mathrm{r}} - \mathrm{T}(\delta)i'_{\mathrm{i}}), \tag{5c}$$

$$u'_{\mathrm{r}} = k_{\mathrm{Pi}}(\rho\mathrm{T}(-\delta)i''_{\mathrm{r}} - i'_{\mathrm{i}}) + k_{\mathrm{Ii}}\mathrm{T}(-\delta)\gamma'' + e' - \frac{\omega^\circ}{\omega_0} l_{\mathrm{i}}\mathrm{T}(\tfrac{\pi}{2})i'_{\mathrm{i}}, \tag{5d}$$

where k_{Pv}, k_{Pi} denote proportional gains for the PI controllers that regulate voltage and current, respectively, $k_{\mathrm{Iv}}, k_{\mathrm{Ii}}$ denote their corresponding integral gains, k_{a} denotes the integrator anti-windup gain of the PI controller that regulates voltage, and c and l_{i} denote the capacitance and inverter-side inductance, respectively, of the LCL filter.

3) LCL Filter: Suppose the inverter synthesizes its reference voltage, u'_{r}, exactly.[3] Then, the LCL filter dynamics are described by

$$\frac{l_{\mathrm{i}}}{\omega_0 r_{\mathrm{i}}}\frac{\mathrm{d}i'_{\mathrm{i}}}{\mathrm{d}t} = \Big(\frac{l_{\mathrm{i}}}{r_{\mathrm{i}}}\mathrm{T}(\tfrac{\pi}{2}) - \mathbb{I}\Big)i'_{\mathrm{i}} + \frac{1}{r_{\mathrm{i}}}(u'_{\mathrm{r}} - e'), \tag{6a}$$

$$\frac{c}{\omega_0}\frac{\mathrm{d}e'}{\mathrm{d}t} = c\mathrm{T}(\tfrac{\pi}{2})e' + (i'_{\mathrm{i}} - i'_{\mathrm{g}}), \tag{6b}$$

$$\frac{l_{\mathrm{g}}}{\omega_0 r_{\mathrm{g}}}\frac{\mathrm{d}i'_{\mathrm{g}}}{\mathrm{d}t} = \Big(\frac{l_{\mathrm{g}}}{r_{\mathrm{g}}}\mathrm{T}(\tfrac{\pi}{2}) - \mathbb{I}\Big)i'_{\mathrm{g}} + \frac{1}{r_{\mathrm{g}}}(e' - v'), \tag{6c}$$

where r_{i} denotes the inverter-side resistance, and r_{g} and l_{g} respectively denote the sum of resistive and inductive elements (from the filter and transmission line) on the grid side.

B. The Primary Controller

The inputs of the primary controller are the capacitor voltage, e', the grid-side current, i'_{g}, the bus voltage, v', the reference active- and reactive-power injecions obtained from a secondary/tertiary control scheme, which we denote by $p^\star$ and $q^\star$, respectively, and the reference voltage magnitude obtained from a tertiary control scheme, which we denote by $E^\star$. The outputs of the primary controller are the reference voltage magnitude, E°, and the reference angular frequency, ω°.

To describe primary-control dynamics, we leverage a *generic primary-control model* [33], that under certain parametric assumptions yields the governing equations corresponding to droop, VSM, or dVOC. Let p and q denote the active- and reactive-power injections at the capacitor terminals of the LCL filter, i.e.,

$$p := (e')^\top i'_{\mathrm{g}}, \quad q := (e')^\top \mathrm{T}(-\tfrac{\pi}{2})i'_{\mathrm{g}}, \tag{7a}$$

and p_{m} and q_{m} denote their low-pass filtered versions, respectively. Then, the dynamics of this generic primary-control model are described by:

$$\frac{\mathrm{d}\delta}{\mathrm{d}t} = \omega^\circ - \omega_0, \tag{7b}$$

$$\tau_{\mathrm{f}}\frac{\mathrm{d}\omega^\circ}{\mathrm{d}t} = \frac{1}{f_{\mathrm{f}}(E^\circ)}\mathbb{e}_1^\top \mathrm{T}(\psi - \tfrac{\pi}{2})\begin{bmatrix} p^\star - p_{\mathrm{m}} \\ q^\star - q_{\mathrm{m}}\end{bmatrix} + \omega_0 - \omega^\circ + \kappa_{\mathrm{d}}\dot{\alpha}, \tag{7c}$$

$$\tau_{\mathrm{v}}\frac{\mathrm{d}E^\circ}{\mathrm{d}t} = \frac{1}{f_{\mathrm{v}}(E^\circ)}\mathbb{e}_2^\top \mathrm{T}(\psi - \tfrac{\pi}{2})\begin{bmatrix} p^\star - p_{\mathrm{m}} \\ q^\star - q_{\mathrm{m}}\end{bmatrix} + f_{\mathrm{e}}(E^\circ, E^\star), \tag{7d}$$

$$\tau_{\mathrm{p}}\frac{\mathrm{d}p_{\mathrm{m}}}{\mathrm{d}t} = -p_{\mathrm{m}} + p, \tag{7e}$$

$$\tau_{\mathrm{q}}\frac{\mathrm{d}q_{\mathrm{m}}}{\mathrm{d}t} = -q_{\mathrm{m}} + q, \tag{7f}$$

$$\frac{1}{\omega_0}\frac{\mathrm{d}\eta}{\mathrm{d}t} = \mathbb{e}_2^\top \mathrm{T}(\alpha)\mathrm{T}(\delta)v', \tag{7g}$$

$$\frac{1}{\omega_0}\frac{\mathrm{d}\alpha}{\mathrm{d}t} = \frac{k_{\mathrm{P}\theta}}{\omega_0}\dot{\eta} + k_{\mathrm{I}\theta}\eta, \tag{7h}$$

where τ_{f}, τ_{v}, τ_{p}, τ_{q}, κ_{d}, $f_{\mathrm{f}}(E^\circ)$, $f_{\mathrm{v}}(E^\circ)$, and $f_{\mathrm{e}}(E^\star, E^\circ)$ denote generic parameters or functions, whose values depend on the adopted primary-control strategy, i.e., droop, VSM, or dVOC; see Table II for the details.

The expressions in (7b)–(7d) outline the relationship between reference voltage (phase, magnitude, and frequency) and output power; (7e)–(7f) capture the low-pass filtering action for the measured active- and reactive-power values; and (7g)–(7h) capture the dynamics of a synchronous reference-frame phase-locked loop (SRF PLL) that is leveraged in the VSM control strategy to compute the mismatch between the bus frequency and the inverter frequency (this mismatch is captured by the term $\dot{\alpha}$ in (7c)). In (7c)–(7d), $\psi \in [0, 2\pi]$ denotes a rotation angle that in steady state determines the nature of the tradeoff between active power and reactive power in the voltage and frequency response of the GFM inverter. In particular, $\psi = \frac{\pi}{2}$ imposes a strong correlation between active power and frequency, and between reactive power and voltage; while $\psi = 0$ does the polar opposite (see, e.g., [26], [33] for details).

The droop control strategy utilizes low-pass-filtered measurements of the active- and reactive-power injections to compute references for angular frequency and voltage magnitude. The reference frequency (voltage) is linearly offset from the nominal-frequency (reference-voltage) by a weighted fraction of the active- and reactive-power deviations from their references, as determined by rotation angle ψ.

[3]This assumption is the basis for developing the inverter averaged model; see [29, pp.32–38].

TABLE II: Parameterizations of the generic primary control model that yield droop, VSM, and dVOC dynamics; see Table I for definitions and base values of the parameters.

	generic-model parameterization							
	τ_{f}	τ_{v}	τ_{p}	τ_{q}	κ_{d}	$f_{\mathrm{f}}(x)$	$f_{\mathrm{v}}(x)$	$f_{\mathrm{e}}(x,y)$
droop	0	0	$\frac{1}{\omega_{\mathrm{c}}}$	$\frac{1}{\omega_{\mathrm{c}}}$	0	d_{f}	d_{v}	$x-y$
VSM	$\frac{m_{\mathrm{f}}}{d_{\mathrm{f}}}$	0	0	$\frac{1}{\omega_{\mathrm{c}}}$	$\frac{d_{\mathrm{d}}}{d_{\mathrm{f}}}$	d_{f}	d_{v}	$x-y$
dVOC	0	$\frac{1}{\omega_0}$	0	0	0	$\frac{x^2}{\omega_0\kappa_1}$	$\frac{x}{\kappa_1}$	$\kappa_2(x^2-y^2)y$

The VSM control strategy utilizes unfiltered measurements of the active power injection and low-pass filtered measurements of the reactive-power injection to compute the reference angular frequency and voltage magnitude. The voltage-magnitude reference is computed identically as in droop control, but for computing the frequency reference, an inertial term (that acts on local frequency) and damping term (that acts on the frequency difference between the inverter and the bus so as to emulate the effect of the damper windings in a synchronous generator) are introduced. The latter requires estimating the frequency of the bus, for which an SRF PLL is leveraged (η and α denote the PLL internal state variable and output phase, respectively).

The dVOC strategy utilizes unfiltered measurements of the active- and reactive-power injections to compute reference values for angular frequency and voltage-magnitude. The frequency reference is offset from its nominal value by a fraction of the active- and reactive-power deviations from their references as determined by rotation angle, ψ; notably, this fraction is a nonlinear function of the voltage-magnitude reference. Distinct from droop and VSM, dVOC includes dynamics for the reference voltage-magnitude E°; this involves nonlinear terms to penalize deviations away from the reference voltage-magnitude $E^{\star}$, as well as deviations of active and reactive power from their references.

III. The Electrical Power Network Model

In this section, we present a graph-theoretic model and a dynamical model for the electric power network. Afterwards, we present a model that describes the terminal relations between the GFM inverter and the network bus it is connected to. We consider $b > 1$ buses, indexed by the elements in the set $\mathcal{B} = \{1, 2, \ldots, b\}$, interconnected via m transmission lines, indexed by the elements in the set $\mathcal{L} = \{1, 2, \ldots, m\}$. Without loss of generality, we assume there is at most one transmission line connecting each pair of buses.

A. Graph-theoretic Network Model

Assign an arbitrary direction for the positive flow of power along each transmission line. Then, the topology of the electrical network with the chosen orientation can be described by a connected directed graph $\mathcal{G} = (\mathcal{V}, \mathcal{E})$, with $\mathcal{V} = \mathcal{B}$ denoting the set of buses, and $\mathcal{E} \subset \mathcal{V} \times \mathcal{V} \setminus \{(k,k) : k \in \mathcal{V}\}$ denoting the set of transmission lines so that $(k,j) \in \mathcal{E}$ if buses k and j are electrically connected, with the flow of power from bus k to bus j assigned to be positive. Let $\mathbb{L}$ denote a one-to-one mapping from $\mathcal{E}$ to $\mathcal{L}$ so that, for each $(k,j) \in \mathcal{E}$, there exists a unique $\ell \in \mathcal{L}$ that satisfies $\ell = \mathbb{L}(k,j)$. Then, we can define a node-to-edge incidence matrix, $M = [m_{k\ell}] \in \{-1, 0, 1\}^{|\mathcal{B}|\times|\mathcal{L}|}$, as follows:

$$\begin{aligned} m_{k\ell} &= 1, && \text{if } \ell = \mathbb{L}(k,j), \quad (k,j) \in \mathcal{E}, \\ m_{k\ell} &= -1, && \text{if } \ell = \mathbb{L}(j,k), \quad (j,k) \in \mathcal{E}, \\ m_{k\ell} &= 0, && \text{otherwise.} \end{aligned}$$

B. Full-order Dynamical Network Model

Consider an electrical network with short transmission lines, rated three-phase power $s_{\mathrm{b},0}$, and rated voltage $e_{\mathrm{b},k}$ for bus $k \in \mathcal{B}$.[4] We represent the network parameters and variables in a per-unit system with base quantities ω_0, $s_{\mathrm{b},0}$, and $e_{\mathrm{b},k}$ at each bus $k \in \mathcal{B}$. The circuit model for each line $\ell \in \mathcal{L}$ is the series connection of a resistance, r_ℓ, and inductance, l_ℓ, both in per unit. Furthermore, we suppose the lines have identical inductance-to-resistance ratio, i.e.,

$$\frac{l_1}{r_1} = \frac{l_2}{r_2} = \cdots = \frac{l_{|\mathcal{L}|}}{r_{|\mathcal{L}|}}.$$

The time constant associated with the line dynamics is denoted by τ_{t}, and the phase angle associated with the line impedance is denoted by φ; these are defined as follows:

$$\tau_{\mathrm{t}} = \frac{l_\ell}{\omega_0 r_\ell}, \ \forall \ell \in \mathcal{L}, \qquad \varphi = \arctan\left(\tau_{\mathrm{t}}\omega_0\right). \tag{8}$$

Let v'_k and i'_k denote the voltage and current injections at bus $k \in \mathcal{B}$, respectively, and let f'_ℓ denote the line current flowing across transmission line ℓ. Then, the dynamics of the line current and the current injection are described by:

$$\tau_{\mathrm{t}}\frac{\mathrm{d}f'_\ell}{\mathrm{d}t} = \left(\tau_{\mathrm{t}}\omega_0 \mathrm{T}(\tfrac{\pi}{2}) - \mathbb{I}\right) f'_\ell + \frac{1}{r_\ell}\sum_{k\in\mathcal{B}} v'_k m_{k\ell}, \tag{9a}$$

$$i'_k = \sum_{\ell\in\mathcal{L}} m_{k\ell} f'_\ell. \tag{9b}$$

Multiplying both sides of (9a) by $m_{k\ell}$ and summing over ℓ yields

$$\begin{aligned} \tau_{\mathrm{t}}\frac{\mathrm{d}}{\mathrm{d}t}\left(\sum_{\ell\in\mathcal{L}} m_{k\ell} f'_\ell\right) = \left(\tau_{\mathrm{t}}\omega_0 \mathrm{T}(\tfrac{\pi}{2}) - \mathbb{I}\right)\sum_{\ell\in\mathcal{L}} m_{k\ell} f'_\ell \\ + \sum_{\ell\in\mathcal{L}} m_{k\ell}\frac{1}{r_\ell}\sum_{k\in\mathcal{B}} v'_k m_{k\ell}. \end{aligned}$$

Substituting (9b) in the above expression, we see that the dynamics of the current injection at bus k are

$$\tau_{\mathrm{t}}\frac{\mathrm{d}i'_k}{\mathrm{d}t} = \left(\tau_{\mathrm{t}}\omega_0 \mathrm{T}(\tfrac{\pi}{2}) - \mathbb{I}\right) i'_k + \sum_{\ell\in\mathcal{L}} m_{k\ell}\frac{1}{r_\ell}\sum_{k\in\mathcal{B}} v'_k m_{k\ell}. \tag{10}$$

Introduce the following matrices

$$\begin{aligned} v'_{\mathcal{B}} &= \left[v'_1,\ v'_2,\ \ldots,\ v'_{|\mathcal{B}|}\right] \in \mathbb{R}^{2\times|\mathcal{B}|}, \\ i'_{\mathcal{B}} &= \left[i'_1,\ i'_2,\ \ldots,\ i'_{|\mathcal{B}|}\right] \in \mathbb{R}^{2\times|\mathcal{B}|}, \end{aligned}$$

[4] A transmission line is typically categorized as *short* if its effective length is less than 50 miles (80 km) [31, p. 208].

$$R = \mathrm{diag}\big(r_1,\ r_2,\ \dots\ ,\ r_{|\mathcal{L}|}\big) \in \mathbb{R}^{|\mathcal{L}|\times|\mathcal{L}|}.$$

Then, we can rewrite (10) in matrix form as follows:

$$\tau_{\mathrm{t}} \frac{\mathrm{d}i'_{\mathcal{B}}}{\mathrm{d}t} = \big(\tau_{\mathrm{t}}\omega_0 \mathrm{T}(\tfrac{\pi}{2}) - \mathbb{I}\big) i'_{\mathcal{B}} + v'_{\mathcal{B}} M R^{-1} M^{\top}. \tag{12}$$

Remark 1. *The general structure of the above model for current dynamics holds for the case of lossless transmission lines as well. In this setting, we collect the inductances of all lines in the matrix*

$$L = \mathrm{diag}\big(l_1,\ l_2,\ \dots\ ,\ l_{|\mathcal{L}|}\big) \in \mathbb{R}^{|\mathcal{L}|\times|\mathcal{L}|}.$$

Then, it follows that the network dynamics can be described by

$$\frac{1}{\omega_0} L \frac{\mathrm{d}i'_{\mathcal{B}}}{\mathrm{d}t} = L\mathrm{T}(\tfrac{\pi}{2}) i'_{\mathcal{B}} + v'_{\mathcal{B}} M M^{\top}. \tag{13}$$

C. Network and Inverter Terminal Relations

Next, we present the relation between the current injection at bus k and the grid-side currents of all GFM inverters connected to bus k, with all relevant variables and parameters translated to a common per-unit system. Consider $n_k \geq 1$ GFM inverters whose output terminals are connected to bus k of an electrical power network with dynamics described by (12). Suppose they have heterogeneous power ratings and homogeneous voltage ratings (since they are parallel connected, we can assume they have the same voltage ratings). The dynamics of each GFM inverter can be described by (4)–(7), with each GFM inverter indexed by superscript $j \in \{1, \dots, n_k\}$. Let $e_{\mathrm{b},k}$ denote the common voltage rating of all n_k inverters, let $s^{(j)}_{\mathrm{b},k}$ denote the rated three-phase power of inverter $j \in \{1, \dots, n_k\}$, and let $s_{\mathrm{b},0}$ denote the rated three-phase power of the electrical network. We make the following assumption on the per-unit model of each GFM inverter.

Assumption 1. *When a group of GFM inverters of the same type are parallel-connected, their per-unit models are identical when: i) the base quantities for each GFM inverter are its rated frequency, rated power, and rated voltage, and ii) they are all initialized with identical per-unit values.*[5]

Suppose the droop-, VSM-, and dVOC-based GFM inverters connected to bus k are indexed by sets $\mathcal{D}_k$, $\mathcal{M}_k$, and $\mathcal{O}_k$, respectively. Then, in the per-unit system with base quantities ω_0, $s_{\mathrm{b},0}$, and $e_{\mathrm{b},k}$, the grid-side current of GFM inverter j, and the net current injection at bus k, are given by $\frac{s^{(j)}_{\mathrm{b},k}}{s_{\mathrm{b},0}} i'^{(j)}_{\mathrm{g},k}$ and $\frac{1}{s_{\mathrm{b},0}} \sum_{j=1}^{n_k} s^{(j)}_{\mathrm{b},k} i'^{(j)}_{\mathrm{g},k}$, respectively; thus, from Assumption 1:

$$\begin{aligned} i'_k &= \tfrac{1}{s_{\mathrm{b},0}} \Big(\sum_{j\in\mathcal{D}_k} s^{(j)}_{\mathrm{b},k} i'^{(j)}_{\mathrm{g},k} + \sum_{j\in\mathcal{M}_k} s^{(j)}_{\mathrm{b},k} i'^{(j)}_{\mathrm{g},k} + \sum_{j\in\mathcal{O}_k} s^{(j)}_{\mathrm{b},k} i'^{(j)}_{\mathrm{g},k} \Big) \\ &= \tfrac{\sum_{j\in\mathcal{D}_k} s^{(j)}_{\mathrm{b},k}}{s_{\mathrm{b},0}} i'^{(\mathcal{D})}_{\mathrm{g},k} + \tfrac{\sum_{j\in\mathcal{M}_k} s^{(j)}_{\mathrm{b},k}}{s_{\mathrm{b},0}} i'^{(\mathcal{M})}_{\mathrm{g},k} + \tfrac{\sum_{j\in\mathcal{O}_k} s^{(j)}_{\mathrm{b},k}}{s_{\mathrm{b},0}} i'^{(\mathcal{O})}_{\mathrm{g},k}, \end{aligned} \tag{14}$$

where $i'^{(\mathcal{D})}_{\mathrm{g},k}$, $i'^{(\mathcal{M})}_{\mathrm{g},k}$, and $i'^{(\mathcal{O})}_{\mathrm{g},k}$ denote the common grid-side currents of all droop-, VSM-, and dVOC-based GFM inverters connected to bus k, respectively.

Remark 2. *Currents i'_k and $i'^{(j)}_{\mathrm{g},k}$, are represented in per-unit systems that have the same base voltage and base frequency, but have base powers $s_{\mathrm{b},0}$ and $s^{(j)}_{\mathrm{b},k}$, respectively.*

IV. Reduced-order Models

In this section, we present the main results of this work, namely, reduced-order models for a diverse and networked group of GFM inverters that preserve the impact of the current-reference limiters. The models are developed via a three-step procedure: (i) for the electrical power network, we apply time-domain Kron reduction, (ii) for parallel-connected GFM inverters we perform dynamic aggregation, and (iii) for the aggregated groups of GFM inverters, we employ singular perturbation analysis. *We wish to preserve the network current dynamics during the model-order reduction process.* The resulting reduced-order models are: 5th-order models for GFM inverters and aggregations, and an algebraic model that describes bus voltages relations for the Kron-reduced network.

A. Network Model Reduction: Time-domain Kron-reduction

Consider the electric power network with dynamics described by (12); each bus has one, several, or no GFM inverters connected to it. Let $\mathcal{I}$ denote the set of buses having one or more GFM inverters connected to them, and let $\mathcal{N}$ denote the set of buses having no GFM inverters connected to them. Partition $M \in \mathbb{R}^{|\mathcal{B}|\times|\mathcal{L}|}$, $i'_{\mathcal{B}} \in \mathbb{R}^{2\times|\mathcal{B}|}$, and $v'_{\mathcal{B}} \in \mathbb{R}^{2\times|\mathcal{B}|}$ as follows:

$$M = \begin{bmatrix} M_{\mathcal{I}} \\ M_{\mathcal{N}} \end{bmatrix},\ i'_{\mathcal{B}} = \begin{bmatrix} i'_{\mathcal{I}} & i'_{\mathcal{N}} \end{bmatrix},\ v'_{\mathcal{B}} = \begin{bmatrix} v'_{\mathcal{I}} & v'_{\mathcal{N}} \end{bmatrix}, \tag{15}$$

where variables with subscripts $\mathcal{I}$ and $\mathcal{N}$ denote sub matrices/vectors whose entries correspond to buses indexed by the elements in the set $\mathcal{I}$ and $\mathcal{N}$, respectively. In what follows, we substitute partitioned versions of M, $i'_{\mathcal{B}}$, and $v'_{\mathcal{B}}$ in (12), while recognizing that buses indexed by $\mathcal{N}$ have no GFM inverters connected to them, so that $i'_{\mathcal{N}} = \frac{\mathrm{d}i'_{\mathcal{N}}}{\mathrm{d}t} = \begin{bmatrix} \mathbb{0}, \mathbb{0} \end{bmatrix}^{\top}$. This yields the following dynamics for current injections at buses indexed by the elements in $\mathcal{I}$:

$$\begin{aligned} \tau_{\mathrm{t}} \frac{\mathrm{d}i'_{\mathcal{I}}}{\mathrm{d}t} &= \big(\tau_{\mathrm{t}}\omega_0 \mathrm{T}(\tfrac{\pi}{2}) - \mathbb{I}\big) i'_{\mathcal{I}} + v'_{\mathcal{I}} M_{\mathcal{I}} R^{-1} M_{\mathcal{I}}^{\top} \\ &\quad + v'_{\mathcal{N}} M_{\mathcal{N}} R^{-1} M_{\mathcal{I}}^{\top}, \end{aligned} \tag{16}$$

and the following algebraic expression for voltages at buses indexed by the elements in $\mathcal{N}$:

$$v'_{\mathcal{N}} = -v'_{\mathcal{I}} M_{\mathcal{I}} R^{-1} M_{\mathcal{N}}^{\top} \big(M_{\mathcal{N}} R^{-1} M_{\mathcal{N}}^{\top}\big)^{-1}. \tag{17}$$

Note that the matrix $M_{\mathcal{N}} R^{-1} M_{\mathcal{N}}^{\top}$ is strictly diagonally dominant, and is therefore invertible (see e.g., [35, Corollary 5.6.17]). Substituting (17) into (16), we can write:

$$\begin{aligned} \tau_{\mathrm{t}} \frac{\mathrm{d}i'_{\mathcal{I}}}{\mathrm{d}t} &= \big(\tau_{\mathrm{t}}\omega_0 \mathrm{T}(\tfrac{\pi}{2}) - \mathbb{I}\big) i'_{\mathcal{I}} + v'_{\mathcal{I}} (M_{\mathcal{I}} R^{-1} M_{\mathcal{I}}^{\top} \\ &\quad - M_{\mathcal{I}} R^{-1} M_{\mathcal{N}}^{\top} \big(M_{\mathcal{N}} R^{-1} M_{\mathcal{N}}^{\top}\big)^{-1} M_{\mathcal{N}} R^{-1} M_{\mathcal{I}}^{\top}). \end{aligned} \tag{18}$$

[5]This assumption implies that parameters of each GFM inverter are designed by multiplying prespecified baseline values by scaling factors that are proportional to the inverter voltage, frequency, and power ratings (see e.g., [34]).

Following from [28, Lemma 2.1], there exists a directed graph $\widetilde{\mathcal{G}} = \big(\mathcal{I}, \widetilde{\mathcal{E}}\big)$ with incidence matrix $\widetilde{M} \in \{-1, 0, 1\}^{|\mathcal{I}|\times|\widetilde{\mathcal{E}}|}$ and diagonal matrix $\widetilde{R} \in \mathbb{R}^{|\widetilde{\mathcal{E}}|\times|\widetilde{\mathcal{E}}|}$ such that

$$\begin{aligned}\widetilde{M}\widetilde{R}^{-1}\widetilde{M}^\top &= M_{\mathcal{I}}R^{-1}M_{\mathcal{I}}^\top \\ &\quad - M_{\mathcal{I}}R^{-1}M_{\mathcal{N}}^\top\big(M_{\mathcal{N}}R^{-1}M_{\mathcal{N}}^\top\big)^{-1}M_{\mathcal{N}}R^{-1}M_{\mathcal{I}}^\top.\end{aligned} \tag{19}$$

Substituting (19) into (18), it follows that the dynamics of the Kron-reduced network model are given by

$$\tau_{\mathrm{t}}\frac{\mathrm{d}i'_{\mathcal{I}}}{\mathrm{d}t} = \big(\tau_{\mathrm{t}}\omega_0\mathrm{T}(\tfrac{\pi}{2}) - \mathbb{I}\big)i'_{\mathcal{I}} + v'_{\mathcal{I}}\widetilde{M}\widetilde{R}^{-1}\widetilde{M}^\top. \tag{20}$$

Remark 3. *There may not exist unique matrices $\widetilde{M}$ and $\widetilde{R}^{-1}$ that satisfy the expression in (19). To address this, we utilized the following iterative approach to guarantee fewer/same number of transmission lines in the Kron-reduced network. The approach includes the following steps:*

1. *Start with $i = 0$, and generate an incidence matrix $\widetilde{M}[i]$ that is based on a complete graph*
2. *Use (19) to solve for $\widetilde{R}^{-1}[i]$ and identify the diagonal elements of $\widetilde{R}^{-1}[i]$ that are zero (or close to zero) and their corresponding edges*
3. *If there are no such diagonal elements, then adopt $\widetilde{M}[i]$ and $\widetilde{R}^{-1}[i]$ as the solutions, otherwise set $i = i + 1$ and go to the next step*
4. *Delete edges identified in step 2 and create $\widetilde{M}[i]$ based on the resulting graph*
5. *Go to step 2*

Remark 4. *Comparing* (20) *with* (12)*, it is evident that the topology of the Kron-reduced network is captured by the incidence matrix, $\widetilde{M}$. The Kron-reduced network comprises $|\mathcal{I}| \le |\mathcal{B}|$ buses that are interconnected via $|\widetilde{\mathcal{E}}| \le |\mathcal{E}|$ transmission lines, with each bus having either one or more GFM inverters connected to it. In effect, the Kron-reduced network only preserves buses that have an inverter connected to them, and it has fewer (or same) number of transmission lines compared to the originating network. Furthermore, transmission lines in the Kron-reduced network are short and have homogeneous inductance-to-resistance ratios, with their resistances and inductances specified in the diagonal matrices $\widetilde{R}$ and $\widetilde{L} = \tau_{\mathrm{t}}\omega_0\widetilde{R}$, respectively.*

B. Inverter Model Reduction: Dynamic Aggregation

Consider three parallel-connected GFM inverters that are based on droop, VSM, and dVOC, respectively. Suppose that they have power ratings, $s_{\mathrm{b},k}^{(\mathcal{D})}$, $s_{\mathrm{b},k}^{(\mathcal{M})}$, and $s_{\mathrm{b},k}^{(\mathcal{O})}$, respectively, and the same voltage rating. Also, suppose that, when their full-order models are per-unitized by using their respective rated frequency, rated power, and rated voltage, the grid-side currents of the droop-, VSM-, and dVOC-based GFM inverters are $i_{\mathrm{g},k}^{\prime(\mathcal{D})}$, $i_{\mathrm{g},k}^{\prime(\mathcal{M})}$ and $i_{\mathrm{g},k}^{\prime(\mathcal{O})}$, respectively. Then, based on (14), the net current injection at bus k is given by

$$i'_k = \tfrac{s_{\mathrm{b},k}^{(\mathcal{D})}}{s_{\mathrm{b},0}} i_{\mathrm{g},k}^{\prime(\mathcal{D})} + \tfrac{s_{\mathrm{b},k}^{(\mathcal{M})}}{s_{\mathrm{b},0}} i_{\mathrm{g},k}^{\prime(\mathcal{M})} + \tfrac{s_{\mathrm{b},k}^{(\mathcal{O})}}{s_{\mathrm{b},0}} i_{\mathrm{g},k}^{\prime(\mathcal{O})}. \tag{21}$$

Comparing (14) and (21), and setting

$$s_{\mathrm{b},k}^{(\mathcal{D})} = \sum_{j\in\mathcal{D}_k} s_{\mathrm{b},k}^{(j)}, \quad s_{\mathrm{b},k}^{(\mathcal{M})} = \sum_{j\in\mathcal{M}_k} s_{\mathrm{b},k}^{(j)}, \quad s_{\mathrm{b},k}^{(\mathcal{O})} = \sum_{j\in\mathcal{O}_k} s_{\mathrm{b},k}^{(j)},$$

it follows that, under Assumption 1, *a group of parallel-connected GFM inverters of the same type can be represented by an aggregate full-order model whose rated power is equal to the total power rating of the GFM inverters.*

C. Network Model Reduction: Elimination Method

Notice that (20) provides a relation between net current injection i'_k and bus voltage v'_k. However, we will find that, by applying the elimination method, (20), (21), and (6c) can be used to develop an algebraic expression that relates the bus voltages to the grid-side currents and the voltage across each LCL filter capacitance; we discuss this next.

Taking advantage of the model aggregation results in Section IV-B, we define the following term which will be used during the model-order reduction steps

$$e'_k = \tfrac{s_{\mathrm{b},k}^{(\mathcal{D})}}{s_{\mathrm{b},0}} e_k^{\prime(\mathcal{D})} + \tfrac{s_{\mathrm{b},k}^{(\mathcal{M})}}{s_{\mathrm{b},0}} e_k^{\prime(\mathcal{M})} + \tfrac{s_{\mathrm{b},k}^{(\mathcal{O})}}{s_{\mathrm{b},0}} e_k^{\prime(\mathcal{O})}, \tag{22}$$

where $\mathcal{D}$, $\mathcal{M}$, and $\mathcal{O}$ are used to identify variables/parameters associated with aggregate models for droop-, VSM-, and dVOC-based GFM inverters, respectively. We make the following assumption on the grid-side resistances and inductances of LCL filters connected to bus k.

Assumption 2. *When models for parallel-connected GFM inverters (based on droop, VSM, and/or dVOC) are per-unitized using their respective rated frequency, rated power, and rated voltage as base quantities, the resulting per-unit values for grid-side resistances (inductances) of all the GFM inverters are identical.*

From (6c), (21), (22), and Assumption 2, we have that the net current injection at bus $k \in \mathcal{I}$ is described by

$$\frac{l_{\mathrm{g},k}}{\omega_0 r_{\mathrm{g},k}}\frac{\mathrm{d}i'_k}{\mathrm{d}t} = \Big(\frac{l_{\mathrm{g},k}}{r_{\mathrm{g},k}}\mathrm{T}(\tfrac{\pi}{2}) - \mathbb{I}\Big)i'_k + \frac{1}{r_{\mathrm{g},k}}(e'_k - \sigma_k v'_k), \tag{23}$$

where, in per-unit, $l_{\mathrm{g},k}$ and $r_{\mathrm{g},k}$ denote the common grid-side inductance and resistance of the GFM inverters, and

$$\sigma_k = \frac{s_{\mathrm{b},k}^{(\mathcal{D})}}{s_{\mathrm{b},0}} + \frac{s_{\mathrm{b},k}^{(\mathcal{M})}}{s_{\mathrm{b},0}} + \frac{s_{\mathrm{b},k}^{(\mathcal{O})}}{s_{\mathrm{b},0}}. \tag{24}$$

Introduce the following matrices

$$e'_{\mathcal{I}} = \Big[e'_1,\ \ldots,\ e'_{|\mathcal{I}|}\Big] \in \mathbb{R}^{2\times|\mathcal{I}|}, \tag{25a}$$

$$\Lambda_{\mathrm{g}} = \mathrm{diag}\Big(\tfrac{l_{\mathrm{g},1}}{\omega_0 r_{\mathrm{g},1}},\ \ldots,\ \tfrac{l_{\mathrm{g},|\mathcal{I}|}}{\omega_0 r_{\mathrm{g},|\mathcal{I}|}}\Big) \in \mathbb{R}^{|\mathcal{I}|\times|\mathcal{I}|}, \tag{25b}$$

$$\Sigma = \mathrm{diag}\big(\sigma_1,\ \ldots,\ \sigma_{|\mathcal{I}|}\big) \in \mathbb{R}^{|\mathcal{I}|\times|\mathcal{I}|}, \tag{25c}$$

$$R_{\mathrm{g}} = \mathrm{diag}\big(r_{\mathrm{g},1},\ \ldots,\ r_{\mathrm{g},|\mathcal{I}|}\big) \in \mathbb{R}^{|\mathcal{I}|\times|\mathcal{I}|}. \tag{25d}$$

Then, from (23) and (25), it follows that the dynamics of current injections into the electrical network, at buses indexed by the set $\mathcal{I}$, can be described by

$$\frac{\mathrm{d}i'_{\mathcal{I}}}{\mathrm{d}t}\Lambda_{\mathrm{g}} = \omega_0\mathrm{T}(\tfrac{\pi}{2})i'_{\mathcal{I}}\Lambda_{\mathrm{g}} - i'_{\mathcal{I}} + (e'_{\mathcal{I}} - v'_{\mathcal{I}}\Sigma)(R_{\mathrm{g}})^{-1}. \tag{26}$$

Using (26) to solve for $\frac{\mathrm{d}i'_{\mathcal{I}}}{\mathrm{d}t} - \omega_0\mathrm{T}(\frac{\pi}{2})i'_{\mathcal{I}}$, and appropriately substituting the result into (20), bus voltages in the Kron-reduced network model can be expressed as the following

linear function of current injections and capacitor voltages:

$$v'_{\mathcal{I}} = \left(i'_{\mathcal{I}} \Big(\frac{1}{\tau_{\mathrm{t}}} \mathbb{I} - \Lambda_{\mathrm{g}}^{-1} \Big) + e'_{\mathcal{I}} (R_{\mathrm{g}} \Lambda_{\mathrm{g}})^{-1} \right) \Pi^{-1}, \tag{27a}$$

where

$$\Pi = \Big(\frac{1}{\tau_{\mathrm{t}}} \widetilde{M} \widetilde{R}^{-1} \widetilde{M}^{\top} + \Sigma (R_{\mathrm{g}} \Lambda_{\mathrm{g}})^{-1} \Big) \in \mathbb{R}^{|\mathcal{I}| \times |\mathcal{I}|} \tag{27b}$$

is strictly diagonally dominant, and therefore invertible, and $i'_{\mathcal{I}}$, $e'_{\mathcal{I}}$ are matrices whose columns: (i) represent weighted sums of grid-side currents and capacitor voltages, respectively (see (21) and (22)), (ii) are balanced three-phase signals represented in the DQ reference frame, and (iii) are associated with each bus of the Kron-reduced network.

Remark 5. *The result in* (27a) *presents a relation between bus voltage, capacitor voltages, and bus current injections. Its derivation results from the fact that all line currents can be expressed as functions of the bus current injections. As a result, the bus voltages, which are functions of line currents and capacitor voltages, can be expressed in terms of the bus current injections and capacitor voltages.*

D. System Model Reduction: Singular Perturbation

Thus far, we have established full-order dynamics of GFM inverters (4)–(7), showed how an aggregate full-order model can be developed for parallel-connected GFM inverters of the same type, and derived a Kron-reduced algebraic model for electrical power networks (27). Next, we perform a systematic model-order reduction on the network and inverter models and present a reduced-order model for GFM inverters that results when the network current dynamics are preserved. In addition to the network current dynamics, the model also captures dynamics of the inverter phase, frequency, reference voltage, and current-reference limiter, as well as the aggregate dynamics of parallel-connected GFM inverters. A few assumptions and preliminaries are required, which are spelled out next.

Following from standard parameter values in [22]–[27], small parameters in the dynamical models can be identified using the following assumption on the GFM inverter connected to bus k of the electrical power network:

Assumption 3. *There exists a small parameter ϵ, as well as constants $\lambda_1, \ldots, \lambda_7 \in (0, 1]$, such that:*

$$\begin{aligned} &\tau_{\mathrm{p},k} = \lambda_1 \epsilon, && \tau_{\mathrm{q},k} = \lambda_2 \epsilon, && \tfrac{c_k}{\omega_0} = \lambda_3 \epsilon, \\ &\tfrac{1}{\omega_0 k_{\mathrm{P}\theta,k}} = \lambda_4 \epsilon, && \tfrac{l_{\mathrm{i},k}}{\omega_0 r_{\mathrm{i},k}} = \lambda_5 \epsilon, && \tfrac{r_{\mathrm{i},k} + k_{\mathrm{Pi},k}}{\omega_0 k_{\mathrm{Ii},k}} = \lambda_6 \epsilon, \\ &\tfrac{k_{\mathrm{Pv},k}}{\omega_0 k_{\mathrm{Iv},k}} = \lambda_7 \epsilon. \end{aligned}$$

The small parameters listed in Assumption 3 represent time constants and gains associated with the primary controller, LCL filter, and PI controller, whose values are a result of controller and filter design specifications. We also require the following assumption on frequency of the GFM inverter(s) connected to bus k of the network.

Assumption 4. *There exists a variable $\lambda_8 \in (-1, 1)$ such that the angular frequency satisfies the constraint*

$$\frac{\omega_k - \omega_0}{\omega_0} = \lambda_8 \epsilon.$$

Primary control strategies of GFM inverters are typically tuned to ensure that a 1 per-unit change in output power injection results in less than 0.05 per-unit change in the angular frequency of the inverter. As a result, GFM inverters would typically satisfy Assumption 4.

The following steps, which are based on singular perturbation analysis as described in [32, pp. 2–22], are used to perform model-order reduction of the full-order dynamical models presented in Sections II and IV-C:

1. The system of equations constituting the GFM inverter models and the Kron-reduced network model are expressed compactly by substituting the algebraic expressions into the differential equations, and the resulting system of equations are represented in the standard singular-perturbation form (see Appendix C for details):
$$\dot{x} = f(x, z, \epsilon), \qquad \epsilon \dot{z} = g(x, z, \epsilon), \tag{28}$$
where $f(\cdot,\cdot,\cdot)$ and $g(\cdot,\cdot,\cdot)$ are continuously differentiable functions of their arguments, $x = \big[x_1^{\top}, \ldots, x_{|\mathcal{I}|}^{\top}\big]^{\top}$, $z = \big[z_1^{\top}, \ldots, z_{|\mathcal{I}|}^{\top}\big]^{\top}$, $x_k = \big[(x_k^{(\mathcal{D})})^{\top}, (x_k^{(\mathcal{M})})^{\top}, (x_k^{(\mathcal{O})})^{\top}\big]^{\top}$, $z_k = \big[(z_k^{(\mathcal{D})})^{\top}, (z_k^{(\mathcal{M})})^{\top}, (z_k^{(\mathcal{O})})^{\top}\big]^{\top}$, with $x_k^{(j)} = \big[\delta_k^{(j)}, \omega_k^{\circ(j)}, E_k^{\circ(j)}, (i_{\mathrm{g},k}^{\prime(j)})^{\top}\big]^{\top}$, $z_k^{(j)} = \big[(p_{\mathrm{m},k}^{(j)})^{\top}, (q_{\mathrm{m},k}^{(j)})^{\top}, \eta_k^{(j)}, \alpha_k^{(j)}, (i_{\mathrm{i},k}^{\prime(j)})^{\top}, (e_k^{\prime(j)})^{\top}, (\phi_k^{\prime\prime(j)})^{\top}, (\gamma_k^{\prime\prime(j)})^{\top}\big]^{\top}$, for $j \in \{\mathcal{D}, \mathcal{M}, \mathcal{O}\}$.
2. The reduced-order model is derived from (28) by: (i) setting $\epsilon = 0$ (this means all parameters listed in Assumptions 3 and 4 are set to zero) (ii) solving for z as a function of x, and (iii) substituting the resulting expression for z into $\dot{x} = f(x, z, \epsilon)$.

Define the following two matrices:

$$\mathrm{A}_{1,k}(x) = \begin{bmatrix} \frac{x}{c_k^2 k_{\mathrm{a},k}^2 (x-1)^2 + x^2} & -\frac{c_k k_{\mathrm{a},k} (x-1)}{c_k^2 k_{\mathrm{a},k}^2 (x-1)^2 + x^2} \\ \frac{c_k k_{\mathrm{a},k} (x-1)}{c_k^2 k_{\mathrm{a},k}^2 (x-1)^2 + x^2} & \frac{x}{c_k^2 k_{\mathrm{a},k}^2 (x-1)^2 + x^2} \end{bmatrix}, \tag{29a}$$

$$\mathrm{A}_{2,k}(x) = \begin{bmatrix} -\frac{c_k^2 k_{\mathrm{a},k} (x-1)}{c_k^2 k_{\mathrm{a},k}^2 (x-1)^2 + x^2} & -\frac{c_k x}{c_k^2 k_{\mathrm{a},k}^2 (x-1)^2 + x^2} \\ \frac{c_k x}{c_k^2 k_{\mathrm{a},k}^2 (x-1)^2 + x^2} & -\frac{c_k^2 k_{\mathrm{a},k} (x-1)}{c_k^2 k_{\mathrm{a},k}^2 (x-1)^2 + x^2} \end{bmatrix}. \tag{29b}$$

Then, the reduced-order dynamical model for a group of $n_k \geq 1$ parallel-connected GFM inverters of the same type, connected to bus $k \in \mathcal{I}$ of an electrical network is depicted in Fig. 2 and is given by:

$$\frac{\mathrm{d}\delta_k}{\mathrm{d}t} = \omega_k^{\circ} - \omega_0, \tag{30a}$$

$$\tau_{\mathrm{f},k} \frac{\mathrm{d}\omega_k^{\circ}}{\mathrm{d}t} = \frac{1}{f_{\mathrm{f},k}(E_k^{\circ})} \mathbb{e}_1^{\top} \mathrm{T}(\psi_k - \tfrac{\pi}{2}) \begin{bmatrix} p_k^{\star} - e_k^{\prime\top} i'_{\mathrm{g},k} \\ q_k^{\star} - e_k^{\prime\top} \mathrm{T}(-\frac{\pi}{2}) i'_{\mathrm{g},k} \end{bmatrix} + \omega_0 - \omega_k^{\circ}, \tag{30b}$$

$$\tau_{\mathrm{v},k} \frac{\mathrm{d}E_k^{\circ}}{\mathrm{d}t} = \frac{1}{f_{\mathrm{v},k}(E_k^{\circ})} \mathbb{e}_2^{\top} \mathrm{T}(\psi_k - \tfrac{\pi}{2}) \begin{bmatrix} p_k^{\star} - e_k^{\prime\top} i'_{\mathrm{g},k} \\ q_k^{\star} - e_k^{\prime\top} \mathrm{T}(-\frac{\pi}{2}) i'_{\mathrm{g},k} \end{bmatrix} + f_{\mathrm{e},k}(E_k^{\star}, E_k^{\circ}), \tag{30c}$$

$$\frac{l_{\mathrm{g},k}}{\omega_0} \frac{\mathrm{d}i'_{\mathrm{g},k}}{\mathrm{d}t} = \Big(l_{\mathrm{g},k} \mathrm{T}(\tfrac{\pi}{2}) - r_{\mathrm{g},k} \mathbb{I} \Big) i'_{\mathrm{g},k} + e'_k - v'_k, \tag{30d}$$

$$e'_k = \frac{\rho_k}{c_k} \mathrm{T}(\tfrac{\pi}{2} - \delta_k) \mathrm{A}_{2,k}(\rho_k) \mathbb{e}_1 E_k^{\circ}$$

This article has been accepted for publication in IEEE Transactions on Power Systems. This is the author's version which has not been fully edited and content may change prior to final publication. Citation information: DOI 10.1109/TPWRS.2022.3229970

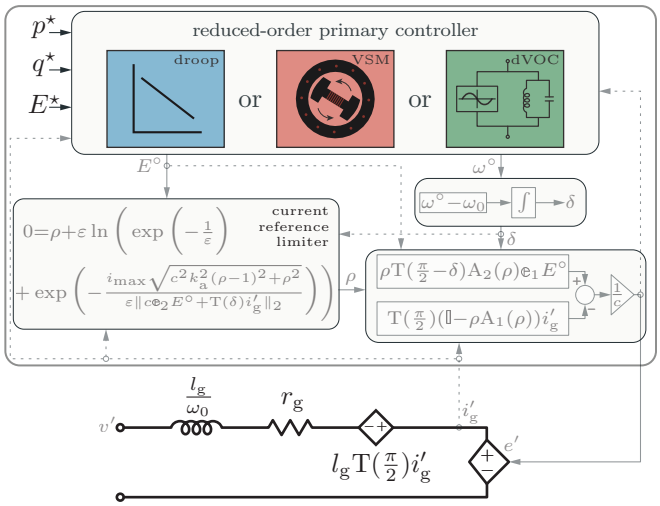

Fig. 2: Reduced-order model for GFM inverters connected to an electrical power network.

$$-\frac{1}{c_k}\mathrm{T}(\tfrac{\pi}{2})(\mathbb{I}-\rho_k \mathrm{A}_{1,k}(\rho_k))i'_{\mathrm{g},k}, \tag{30e}$$

$$0=\rho_k+\varepsilon\ln\left(\exp\left(-\frac{1}{\varepsilon}\right)+\exp\left(-\frac{i_{\max}\sqrt{c_k^2k_{\mathrm{a},k}^2(\rho_k-1)^2+{\rho_k}^2}}{\varepsilon\|c_k\mathbb{e}_2E_k^\circ+\mathrm{T}(\delta_k)i'_{\mathrm{g},k}\|_2}\right)\right), \tag{30f}$$

and from (27), the reduced-order model for the network is

$$v'_{\mathcal{I}}=\left(i'_{\mathcal{I}}\left(\mathbb{I}\tfrac{1}{\tau_{\mathrm{t}}}-\Lambda_{\mathrm{g}}^{-1}\right)+e'_{\mathcal{I}}(R_{\mathrm{g}}\Lambda_{\mathrm{g}})^{-1}\right)\Pi^{-1}, \tag{30g}$$

where, Π is described by (27b), the k-th column of matrix $v'_{\mathcal{I}}$ is v'_k, and the k-th column of matrices $i'_{\mathcal{I}}$ and $e'_{\mathcal{I}}$ are described by (21) and (22), respectively.

Remark 6. *Consider the special/simplifying case where the current-reference limiter is inactive. In this case, we note that* $\rho_k = 1$, *and* $A_{1,k}(\rho_k) = A_{1,k}(1) = \mathbb{I}$, $A_{2,k}(\rho_k) = A_{2,k}(1) = \begin{bmatrix} 0 & -c_k \\ c_k & 0 \end{bmatrix}$. *The dynamics described by* (30b)–(30c) *are preserved, but the expressions in* (30e) *and* (30f) *transform to*

$$e'_k = \mathrm{T}(-\delta_k)\mathbb{e}_1E_k^\circ, \qquad \rho_k = 1. \tag{31}$$

V. Numerical Results

We provide two sets of numerical case studies to validate the approach. Simulation results for a modified IEEE 14-bus network with aggregations of inverters at some buses (see Fig. 3) provide an in-depth examination of the accuracy of the original and reduced-order models through large-signal transients that activate current-limiting action. Simulation results for a modified IEEE 118-bus network (see Fig. 5) demonstrate scalability of the approach without compromising accuracy to large networks.

In each case we will note a marked reduction in computation effort since the reduced-order models are described by fewer dynamic states at the network and device level. Let $\mathcal{I}_{\mathcal{D}}/\mathcal{I}_{\mathcal{M}}/\mathcal{I}_{\mathcal{O}}$ respectively denote the set of all buses with droop/VSM/dVOC-based GFM inverters connected to them. At bus k, let $\mathcal{D}_k/\mathcal{M}_k/\mathcal{O}_k$ denote the sets of all parallel-connected GFM inverters based on droop/VSM/dVOC, respectively. Based on the analytical results presented in this paper, we expect that at each bus comprising droop/VSM/dVOC-based GFM inverters, our proposed approach will reduce the model-order by a factor of $\frac{13|\mathcal{D}_k|}{3}/\frac{15|\mathcal{M}_k|}{4}/3|\mathcal{O}_k|$, respectively. Note also from Remark 3 that the approach adopted for time-domain model reduction targets a reduction in the number of lines in the reduced network, thereby guaranteeing computational savings on that front as well. (It is not straightforward to precisely quantify the reduction in the number of states in this case since it is network and parameter dependent.)

A. The IEEE 14-bus network

We consider the IEEE 14-bus network depicted in Fig. 3. The electrical power network comprises buses indexed by elements in the set $\mathcal{I} = \{1, 2, \ldots, 5\}$, which have at least one GFM inverter connected to them, buses indexed by the elements in the set $\mathcal{N} = \{6, 7, \ldots, 14\}$, which have no GFM inverters or loads connected to them, and lines indexed by the elements in the set $\mathcal{L} = \{1, 2, \ldots, 20\}$, which interconnect the buses. Parameter values are provided in the Appendix.

Time-domain Kron reduction is employed to reduce the IEEE 14-bus system to a 5-bus system with buses indexed by the elements in the set $\mathcal{I} = \{1, 2, \ldots, 5\}$ and lines indexed by the elements in the set $\widetilde{\mathcal{L}} = \{1, 2, \ldots, 10\}$. (Also depicted in Fig. 3.) Full-order models for the droop-, VSM-, and dVOC-based GFM inverters are reduced from 13th-, 15th-, and 12th-order models to 2rd-, 3th- and 3th-order models, respectively, and full-order models for the parallel-connected GFM inverters at buses 3, 4, and 5 of the 14-bus system are reduced from 56th-, 36th-, and 26th-order models to 5th-, 3rd, and 2nd-order models, respectively. Table III lists the total number of dynamic states corresponding to the network and the inverters in the original and reduced-order models.

Figure 4 illustrates the active- and reactive-power outputs, current magnitude, voltage magnitude, and frequency at buses 1–5 over a 15 s period during which the active- and reactive-power references of the inverters, $p_k^\star$, $q_k^\star$, $k \in \{1, 2, 3, 4, 5\}$, are varied as indicated by the blue lines in the p_k and q_k plots. (If more than one GFM inverter is connected to a bus, e.g., on bus 3, then every GFM inverter receives an equal share of the power setpoint.) Current limits for each of the buses are shown in dashed blue lines in the current-waveform plots. Results corresponding to the full-order IEEE 14-bus network are plotted as red-colored lines; those corresponding to the reduced system are shown as black lines. The match between the two establishes the validity of the reduced-order models. The match holds even during periods when the current limits are breached and the current limiters are active. Table III also lists the computation time for the two simulation runs. We note a drastic reduction in computation time for the reduced-order model since the number of states are much lower.

This article has been accepted for publication in IEEE Transactions on Power Systems. This is the author's version which has not been fully edited and content may change prior to final publication. Citation information: DOI 10.1109/TPWRS.2022.3229970

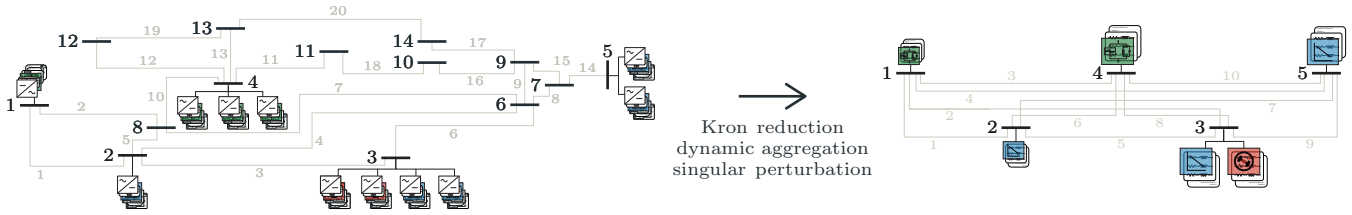

(a) The IEEE 14-bus system (b) The reduced 5-bus system

Fig. 3: The IEEE 14-bus test system and its equivalent Kron-reduced model. The test system comprises *14 buses* (—), and *20 lines* (—) whereas the Kron-reduced model comprises *5 buses* (—), and *10 lines* (—). Notice also that the reduced-order network involves lower-order models of inverter dynamics for each primary-control type.

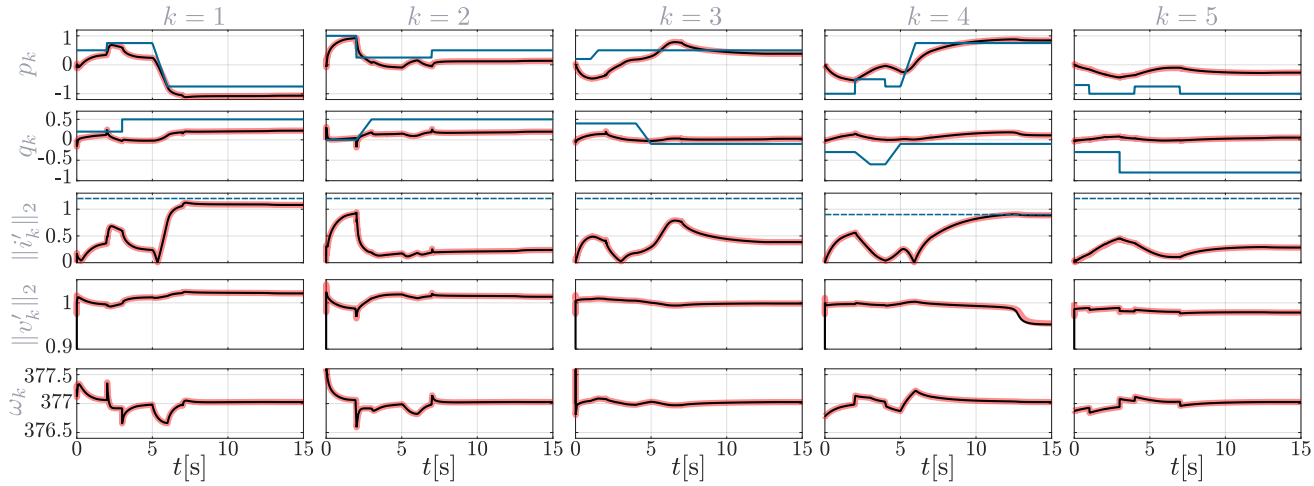

Fig. 4: Numerical simulation results of the IEEE 14-bus network and the Kron-reduced network, visualizing the active power exchange, reactive power exchange, current magnitude, voltage magnitude and frequency at every boundary bus. Measurements of the full-order IEEE 14-bus network are displayed as red-colored lines, measurements of the Kron-reduced network as black-colored lines. Active and reactive power set-points, i.e., $p^\star$ and $q^\star$, are depicted as blue-colored lines.

B. The IEEE 118*-bus network*

We consider the IEEE 118-bus network depicted in Fig. 5. The electrical power network comprises buses indexed by elements in the set $\mathcal{I} = \{1, 2, \ldots, 25\}$, which have a single GFM inverter connected to them, buses indexed by the elements in the set $\mathcal{N} = \{26, 27, \ldots, 118\}$, which have no GFM inverters or loads connected to them, and lines indexed by the elements in the set $\mathcal{L} = \{1, 2, \ldots, 186\}$, which interconnect the buses. Parameter values are provided in the Appendix.

Time-domain Kron reduction is employed to reduce the IEEE 118-bus system to a 25-bus system with buses indexed by the elements in the set $\mathcal{I} = \{1, 2, \ldots, 25\}$ and lines indexed by the elements in the set $\widetilde{\mathcal{L}} = \{1, 2, \ldots, 151\}$. (Also depicted in Fig. 5.). Table IV lists the total number of dynamic states corresponding to the network and the inverters in the original and reduced-order models.

Figure 6 illustrates the active power outputs, current magnitude, and voltage magnitude at buses 1–25 over a 4 s period during which the active power references of the inverters, i.e., $p_k^\star$, $k \in \{1, \ldots, 25\}$, are varied as indicated by the blue lines in the p_k plots. Results corresponding to the full-order IEEE 118-bus network are plotted as red-colored lines; those corresponding to the reduced system are shown as black-colored lines. The match between the two establishes the validity of the reduced-order models. Table IV also lists the computation time for the two simulation runs. Again, we obtain a drastic reduction in computation time for the reduced-order model since the number of states are lower. Broadly, this result establishes the scalability of the proposed approach.

VI. Concluding Remarks & Future Work

This work outlined reduced-order models for grid-forming inverter-based power networks. Compared to previous efforts for model reduction, our proposed models retain the network interactions in the time domain and the effects of the current-reference limiter in the reduced-order models. The approach also applies to a wide range of primary-control methods that have received attention in the GFM space recently. Uniquely, the reduced-order models preserve structure of the originating models at the resource and network levels. This makes the results accessible and readily implementable in simulation software. Simulation results for the IEEE 14- and 118-bus networks establish scalability of the proposed approach, and indicate that the proposed reduced-order models require an order-of-magnitude less computational effort to produce results with the same order-of-magnitude accuracy as the full-order models.

As part of future work, we point out that the results in [36] can be leveraged to extend the time-domain Kron reduction

TABLE III: Numerical results: IEEE 14-bus network.

	Full-order network	Reduced network
# Dynamic inverter-states	143	15
# Dynamic line-states	60	30
# Total dynamic states	203	45
Total computation time	313.4 s	149.2 s

TABLE IV: Numerical results: IEEE 118-bus network.

	Full-order network	Reduced-order network
# Dynamic inverter-states	332	67
# Dynamic line-states	558	453
# Total dynamic states	890	520
Total computation time	325.8 s	159.5 s

method applied for the network dynamics to settings where the l/r ratios of the lines are not all identical. Application of the proposed methods to practical utility-scale installations that involve collections of wind or solar resources and plant controllers is also a pertinent direction for future work. Finally, methods proposed for model reduction and dynamic aggregation could be extended to unbalanced systems.

APPENDIX

A. GFM Inverter Parameters

Following from Assumption 1, all GFM inverters in the network have the same per-unit values for each parameter. Accordingly, common model parameters for all GFM inverter models are: $\varepsilon = 0.02$, $i_{\max} = 1.2$, $k_{\rm a} = 0.035$, $\psi = \pi/2$, $E^\star = 1$, $\omega_0 = 2\pi 60$, $k_{{\rm P}\theta} = 1$, $k_{{\rm I}\theta} = 0.0028$, $l_{\rm i} = 0.02$, $l_{\rm g} = 0.02$, $c = 0.11$, $r_{\rm i} = 0.014$, $r_{\rm g} = 0.014$, $k_{\rm Pv} = 1.45$, $k_{\rm Iv} = 10.29$, $k_{\rm Pi} = 0.98$, $k_{\rm Ii} = 0.69$, $\kappa_1 = 0.003$, $\kappa_2 = 0.046$, $d_{\rm f} = 0.8$, $d_{\rm v} = 25$, $d_{\rm d} = 0.005$, $m_{\rm f} = 0.01$, $\omega_{\rm c} = 125.7$, with the subscript "k" omitted to contain notational burden.

1) The IEEE 14-bus network: The rated power and voltages for the GFM inverters are: $s_{{\rm b},1} = 15\,{\rm kVA}$, $s_{{\rm b},2} = 10\,{\rm kVA}$, $s_{{\rm b},3}^{(1)} = 4\,{\rm kVA}$, $s_{{\rm b},3}^{(2)} = 5\,{\rm kVA}$, $s_{{\rm b},3}^{(3)} = 6\,{\rm kVA}$, $s_{{\rm b},3}^{(4)} = 7\,{\rm kVA}$, $s_{{\rm b},4}^{(1)} = 4\,{\rm kVA}$, $s_{{\rm b},4}^{(2)} = 5\,{\rm kVA}$, $s_{{\rm b},4}^{(3)} = 6\,{\rm kVA}$, $s_{{\rm b},5}^{(1)} = 4\,{\rm kVA}$, $s_{{\rm b},5}^{(2)} = 5\,{\rm kVA}$, $e_{{\rm b},1} = e_{{\rm b},2} = \cdots = e_{{\rm b},5} = 408\,{\rm V}$.

2) The IEEE 118-bus network: The rated powers and voltages for the GFM inverters are: $s_{{\rm b},1} = 15\,{\rm kVA}$, $s_{{\rm b},2} = 10\,{\rm kVA}$, $s_{{\rm b},3} = 4\,{\rm kVA}$, $s_{{\rm b},4} = 5\,{\rm kVA}$, $s_{{\rm b},5} = 6\,{\rm kVA}$, $s_{{\rm b},6} = 7\,{\rm kVA}$, $s_{{\rm b},7} = 4\,{\rm kVA}$, $s_{{\rm b},8} = 5\,{\rm kVA}$, $s_{{\rm b},9} = 6\,{\rm kVA}$, $s_{{\rm b},10} = 4\,{\rm kVA}$, $s_{{\rm b},11} = 15\,{\rm kVA}$, $s_{{\rm b},12} = 10\,{\rm kVA}$, $s_{{\rm b},13} = 4\,{\rm kVA}$, $s_{{\rm b},14} = 5\,{\rm kVA}$, $s_{{\rm b},15} = 6\,{\rm kVA}$, $s_{{\rm b},16} = 7\,{\rm kVA}$, $s_{{\rm b},17} = 4\,{\rm kVA}$, $s_{{\rm b},18} = 5\,{\rm kVA}$, $s_{{\rm b},19} = 6\,{\rm kVA}$, $s_{{\rm b},20} = 4\,{\rm kVA}$, $s_{{\rm b},21} = 5\,{\rm kVA}$, $s_{{\rm b},22} = 10\,{\rm kVA}$, $s_{{\rm b},23} = 4\,{\rm kVA}$, $s_{{\rm b},24} = 5\,{\rm kVA}$, $s_{{\rm b},25} = 6\,{\rm kVA}$, $e_{{\rm b},1} = e_{{\rm b},2} = \cdots = e_{{\rm b},25} = 408\,{\rm V}$.

B. Network Parameters

1) The IEEE 14-bus network: The rated three-phase power of the network is $s_{{\rm b},0} = 100$ MVA, and the time constant associated with the transmission-line dynamics is $\tau_{\rm t} = 1 \times 10^{-3}\,{\rm s\,rad^{-1}}$. The per-unit line inductances are obtained from the line parameter data presented in [37] for the IEEE-14 bus network, and the corresponding line resistances are computed by dividing the inductances by $\tau_{\rm t}\omega_0$.

The per-unit line resistances of the Kron-reduced 5-bus network are: $\widetilde{r}_1 = 0.14$, $\widetilde{r}_2 = 3.91$, $\widetilde{r}_3 = 2.89$, $\widetilde{r}_4 = 9.4$, $\widetilde{r}_5 = 0.36$, $\widetilde{r}_6 = 1.27$, $\widetilde{r}_7 = 2.84$, $\widetilde{r}_8 = 2.84$, $\widetilde{r}_9 = 4.51$, and $\widetilde{r}_{10} = 2.04$. The corresponding per-unit line inductances are computed by multiplying the resistance values by $\tau_{\rm t}\omega_0$.

2) The IEEE 118-bus network: The rated three-phase power of the network is $s_{{\rm b},0} = 500$ MVA, and the time constant associated with the transmission-line dynamics is $\tau_{\rm t} = 2.04 \times 10^{-3}\,{\rm s\,rad^{-1}}$. The per-unit line inductances are obtained from the line parameter data presented in [38] for the IEEE-118 bus network, and the corresponding line resistances are computed by dividing the inductances by $\tau_{\rm t}\omega_0$.

The per-unit line conductances of the Kron-reduced 25-bus network are computed by generating an incidence matrix $\widetilde{M}$ using Fig. 5b, and solving for $\widetilde{R}^{-1}$ (the diagonal elements of the matrix correspond to the per-unit line conductances). The corresponding per-unit line inductances are computed by dividing $\tau_{\rm t}\omega_0$ by the line conductance.

C. Representing the Full-order Model in Standard Form

The grid-forming inverter network dynamics introduced in Sections II and III can be expressed in standard form for singular perturbation by:

(i) substituting (27b) into (27a) to give:

$$v_{\mathcal{I}}' = \Big(i_{\mathcal{I}}'\Big(\frac{1}{\tau_{\rm t}}\mathbb{I} - \Lambda_{\rm g}^{-1}\Big) + e_{\mathcal{I}}'(R_{\rm g}\Lambda_{\rm g})^{-1}\Big)\Big(\frac{1}{\tau_{\rm t}}\widetilde{M}\widetilde{R}^{-1}\widetilde{M}^{\top} + \Sigma(R_{\rm g}\Lambda_{\rm g})^{-1}\Big)^{-1}, \tag{32}$$

(ii) substituting (5b) into (5a), (5c), (5d), and (4) to give

$$\frac{1}{\omega_0}\frac{{\rm d}\phi''}{{\rm d}t} = (\rho-1)k_{\rm a}\big(k_{\rm Pv}(\mathbb{e}_1 E^\circ - {\rm T}(\delta)e') + k_{\rm Iv}\phi'' + {\rm T}(\delta)i_{\rm g}' - \frac{\omega^\circ}{\omega_0}c{\rm T}(\delta+\tfrac{\pi}{2})e'\big) + \mathbb{e}_1 E^\circ - {\rm T}(\delta)e', \tag{33a}$$

$$\frac{1}{\omega_0}\frac{{\rm d}\gamma''}{{\rm d}t} = \rho\big(k_{\rm Pv}(\mathbb{e}_1 E^\circ - {\rm T}(\delta)e') + k_{\rm Iv}\phi'' + {\rm T}(\delta)i_{\rm g}' - \frac{\omega^\circ}{\omega_0}c{\rm T}(\delta+\tfrac{\pi}{2})e'\big) - {\rm T}(\delta)i_{\rm i}', \tag{33b}$$

$$u_{\rm r}' = \rho k_{\rm Pi}\big(k_{\rm Pv}({\rm T}(-\delta)\mathbb{e}_1 E^\circ - e') - \frac{\omega^\circ}{\omega_0}{\rm T}(\tfrac{\pi}{2})ce' + k_{\rm Iv}{\rm T}(-\delta)\phi'' + i_{\rm g}'\big) + e' + k_{\rm Ii}{\rm T}(-\delta)\gamma'' - \big(k_{\rm Pi}\mathbb{I} + \frac{\omega^\circ}{\omega_0}{\rm T}(\tfrac{\pi}{2})l_{\rm i}\big)i_{\rm i}', \tag{33c}$$

$$\rho = -\varepsilon\ln\Bigg(\exp\Big(-\frac{1}{\varepsilon}\Big) + \exp\Big(-i_{\max} \div \varepsilon\Big\|k_{\rm Pv}(\mathbb{e}_1 E^\circ - {\rm T}(\delta)e') + k_{\rm Iv}\phi''$$

This article has been accepted for publication in IEEE Transactions on Power Systems. This is the author's version which has not been fully edited and content may change prior to final publication. Citation information: DOI 10.1109/TPWRS.2022.3229970

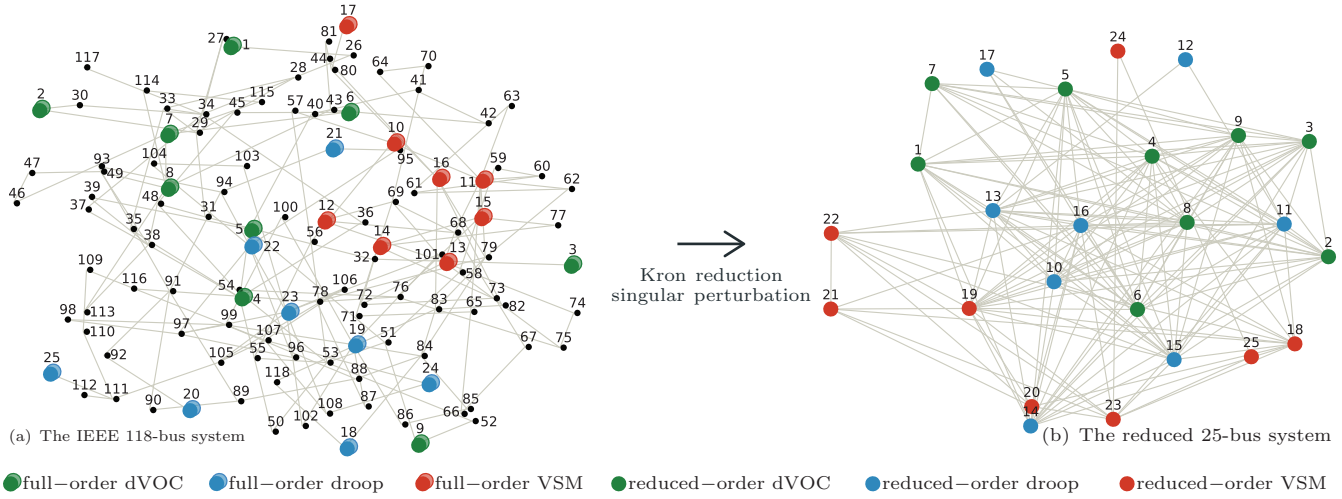

Fig. 5: The test system and its equivalent Kron-reduced network model. The test system comprises *118 buses* and *186 lines*, and the Kron-reduced model comprises *25 buses*, and *151 lines*.

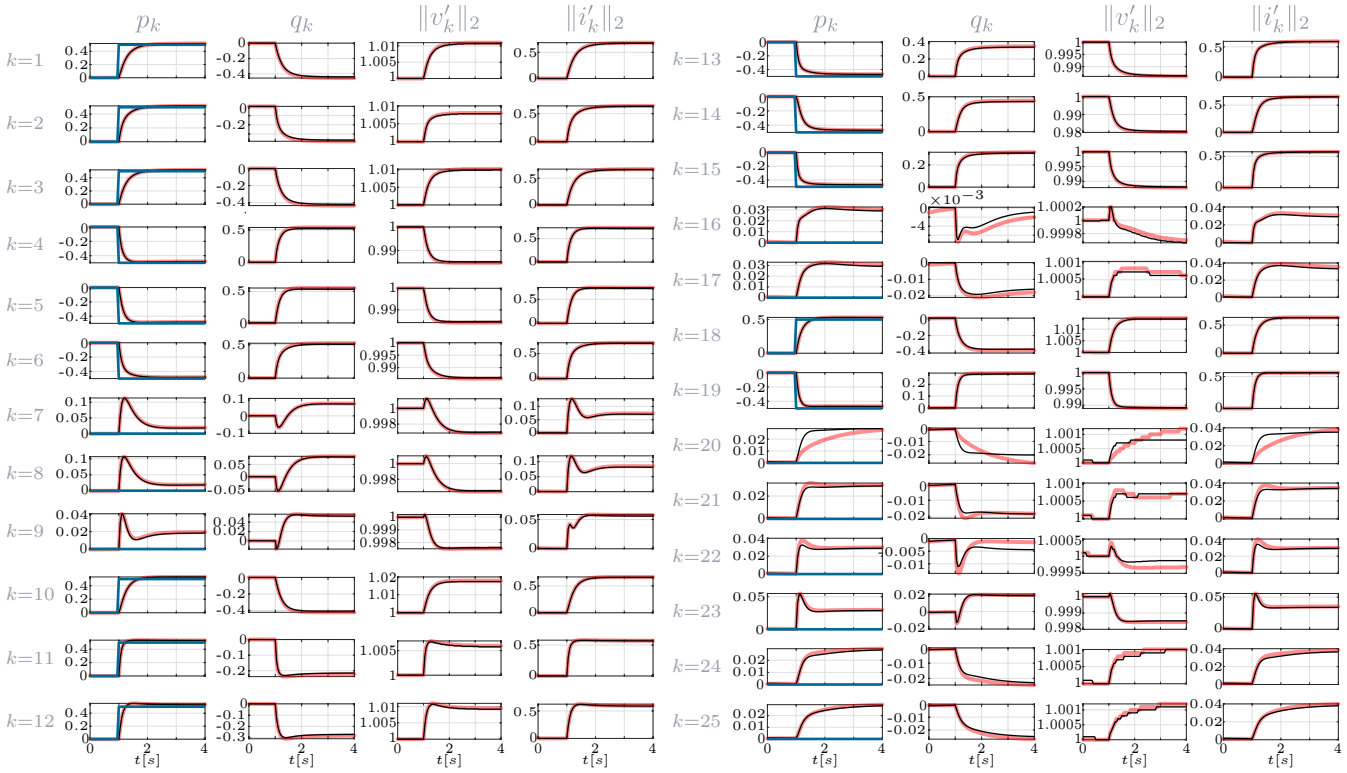

Fig. 6: Numerical simulation results of the IEEE 118-bus network and the 25-bus Kron-reduced network visualizing the active power exchange, reactive power exchange, current magnitude, and voltage magnitude at every boundary bus. Measurements of the full-order IEEE 118-bus network are displayed as red-colored lines, measurements of the Kron-reduced network as black-colored lines. Active power set-points, i.e., $p^\star$, are depicted as blue-colored lines.

$$+ \mathrm{T}(\delta) i'_{\mathrm{g}} - \frac{\omega^\circ}{\omega_0} c \mathrm{T}(\delta + \tfrac{\pi}{2}) e' \big\|_2 \Big) \Big), \tag{33d}$$

(iii) substituting (33c) into (6a) to give

$$\frac{l_{\mathrm{i}}}{\omega_0 r_{\mathrm{i}}} \frac{\mathrm{d}i'_{\mathrm{i}}}{\mathrm{d}t} = \Big(\frac{\omega_0 - \omega^\circ}{\omega_0} \frac{l_{\mathrm{i}}}{r_{\mathrm{i}}} \mathrm{T}(\tfrac{\pi}{2}) - \frac{r_{\mathrm{i}} + k_{\mathrm{Pi}}}{r_{\mathrm{i}}} \mathbb{I} \Big) i'_{\mathrm{i}} + \rho \frac{k_{\mathrm{Pi}}}{r_{\mathrm{i}}} \big(k_{\mathrm{Pv}} (\mathrm{T}(-\delta) \mathbb{e}_1 E^\circ - e') - \frac{\omega^\circ}{\omega_0} \mathrm{T}(\tfrac{\pi}{2}) c e'$$

$$+ k_{\mathrm{Iv}} \mathrm{T}(-\delta) \phi'' + i'_{\mathrm{g}} \big) + \frac{k_{\mathrm{Ii}}}{r_{\mathrm{i}}} \mathrm{T}(-\delta) \gamma''. \tag{33e}$$

(iv) at each bus, an aggregate model is used to represent the dynamics of parallel-connected GFM inverters of the same type

(v) substituting expressions for ρ_k and v'_k, obtained from (4) and (32), respectively, into the full-order model and utilizing Assumption 3 to express the resulting system of equations as a function of a small parameter ϵ. The ag-

gregate full-order model for a group of $n_k \geq 1$ parallel-connected GFM inverters of the same type, connected to bus $k \in \mathcal{I}$ of an electrical network is given by:[6]

$$\frac{\mathrm{d}\delta_k}{\mathrm{d}t} = \omega_k^\circ - \omega_0, \tag{34a}$$

$$\frac{\mathrm{d}\omega_k^\circ}{\mathrm{d}t} = \frac{1}{f_{\mathrm{f},k}(E_k^\circ)}\frac{1}{\tau_{\mathrm{f},k}}\mathbb{e}_1^\top \mathrm{T}(\psi_k - \tfrac{\pi}{2})\begin{bmatrix} p_k^\star - p_{\mathrm{m},k} \\ q_k^\star - q_{\mathrm{m},k}\end{bmatrix} + \frac{1}{\tau_{\mathrm{f},k}}(\omega_0 - \omega_k^\circ) + \omega_0\frac{\kappa_{\mathrm{d},k}}{\tau_{\mathrm{f},k}}\big(k_{\mathrm{I}\theta,k}\eta_k + k_{\mathrm{P}\theta,k}\mathbb{e}_2^\top \mathrm{T}(\alpha_k + \delta_k)v_k'\big), \tag{34b}$$

$$\frac{\mathrm{d}E_k^\circ}{\mathrm{d}t} = \frac{1}{f_{\mathrm{v},k}(E_k^\circ)}\frac{1}{\tau_{\mathrm{v},k}}\mathbb{e}_2^\top \mathrm{T}(\psi_k - \tfrac{\pi}{2})\begin{bmatrix} p_k^\star - p_{\mathrm{m},k} \\ q_k^\star - q_{\mathrm{m},k}\end{bmatrix} + \frac{1}{\tau_{\mathrm{v},k}} f_{\mathrm{e},k}(E_k^\star, E_k^\circ), \tag{34c}$$

$$\frac{\mathrm{d}i_{\mathrm{g},k}'}{\mathrm{d}t} = \Big(\omega_0 \mathrm{T}(\tfrac{\pi}{2}) - \frac{\omega_0 r_{\mathrm{g},k}}{l_{\mathrm{g},k}}\mathbb{I}\Big)i_{\mathrm{g},k}' + \frac{\omega_0}{l_{\mathrm{g},k}}(e_k' - v_k'), \tag{34d}$$

$$\frac{1}{\omega_0}\frac{\mathrm{d}\eta_k}{\mathrm{d}t} = \mathbb{e}_2^\top \mathrm{T}(\alpha_k + \delta_k)v_k', \tag{34e}$$

$$\frac{1}{\omega_0}\frac{\mathrm{d}\alpha_k}{\mathrm{d}t} = k_{\mathrm{P}\theta,k}\mathbb{e}_2^\top \mathrm{T}(\alpha_k + \delta_k)v_k' + k_{\mathrm{I}\theta,k}\eta_k, \tag{34f}$$

$$\frac{1}{\omega_0}\frac{\mathrm{d}\phi_k''}{\mathrm{d}t} = (\rho_k - 1)k_{\mathrm{a},k}\Big(k_{\mathrm{Pv},k}(\mathbb{e}_1 E_k^\circ - \mathrm{T}(\delta_k)e_k') - \big(1 + \epsilon\lambda_8\big)c_k \mathrm{T}(\delta_k + \tfrac{\pi}{2})e_k' + k_{\mathrm{Iv},k}\phi_k'' + \mathrm{T}(\delta_k)i_{\mathrm{g},k}'\Big) + \mathbb{e}_1 E_k^\circ - \mathrm{T}(\delta_k)e_k', \tag{34g}$$

$$\frac{1}{\omega_0}\frac{\mathrm{d}\gamma_k''}{\mathrm{d}t} = \rho_k\big(k_{\mathrm{Pv},k}(\mathbb{e}_1 E_k^\circ - \mathrm{T}(\delta_k)e_k') + k_{\mathrm{Iv},k}\phi_k'' - \big(1 + \epsilon\lambda_8\big)c_k \mathrm{T}(\delta_k + \tfrac{\pi}{2})e_k'\big) + \mathrm{T}(\delta_k)\big(i_{\mathrm{g},k}' - i_{\mathrm{i},k}'\big), \tag{34h}$$

$$\rho_k = -\varepsilon \ln\Bigg(\exp\Big(-\frac{1}{\varepsilon}\Big) + \exp\Big(-i_{\max} \div \varepsilon\big\|k_{\mathrm{Pv},k}(\mathbb{e}_1 E_k^\circ - \mathrm{T}(\delta)e_k') + k_{\mathrm{Iv},k}\phi'' - \frac{\omega_k^\circ}{\omega_0}c_k \mathrm{T}(\delta_k + \tfrac{\pi}{2})e_k' + \mathrm{T}(\delta_k)i_{\mathrm{g},k}'\big\|_2\Big)\Bigg), \tag{34i}$$

$$\epsilon\lambda_6\frac{\mathrm{d}i_{\mathrm{i},k}'}{\mathrm{d}t} = \Big(\epsilon\lambda_8\frac{l_{\mathrm{i},k}}{r_{\mathrm{i},k}}\mathrm{T}(\tfrac{\pi}{2}) - \frac{r_{\mathrm{i},k} + k_{\mathrm{Pi},k}}{r_{\mathrm{i},k}}\mathbb{I}\Big)i_{\mathrm{i},k}' + \frac{k_{\mathrm{Ii},k}}{r_{\mathrm{i},k}}\mathrm{T}(-\delta_k)\gamma_k'' + \rho_k\frac{k_{\mathrm{Pi},k}}{r_{\mathrm{i},k}}\Big(i_{\mathrm{g},k}' - \big(1 + \epsilon\lambda_8\big)\mathrm{T}(\tfrac{\pi}{2})c_k e_k' + k_{\mathrm{Iv},k}\mathrm{T}(-\delta_k)\phi_k'' + k_{\mathrm{Pv},k}(\mathrm{T}(-\delta_k)\mathbb{e}_1 E_k^\circ - e_k')\Big), \tag{34j}$$

$$\epsilon\lambda_4\frac{\mathrm{d}e_k'}{\mathrm{d}t} = c_k \mathrm{T}(\tfrac{\pi}{2})e_k' + i_{\mathrm{i},k}' - i_{\mathrm{g},k}', \tag{34k}$$

$$\epsilon\lambda_1\frac{\mathrm{d}p_{\mathrm{m},k}}{\mathrm{d}t} = -p_{\mathrm{m},k} + {e_k'}^\top i_{\mathrm{g},k}', \tag{34l}$$

$$\epsilon\lambda_2\frac{\mathrm{d}q_{\mathrm{m},k}}{\mathrm{d}t} = -q_{\mathrm{m},k} + {e_k'}^\top \mathrm{T}(-\tfrac{\pi}{2})i_{\mathrm{g},k}', \tag{34m}$$

[6]Due to page constraints, we avoid explicitly presenting the expressions that result when ρ_k and v_k' are eliminated from the full-order model. Instead, we include (4) and (32) as part of the full-order model.

and the bus voltages v_k', $\forall k \in \mathcal{I}$, are described by the relation

$$v_{\mathcal{I}}' = \Big(i_{\mathcal{I}}'\Big(\frac{1}{\tau_{\mathrm{t}}}\mathbb{I} - \Lambda_{\mathrm{g}}^{-1}\Big) + e_{\mathcal{I}}'(R_{\mathrm{g}}\Lambda_{\mathrm{g}})^{-1}\Big)\Big(\frac{1}{\tau_{\mathrm{t}}}\widetilde{M}\widetilde{R}^{-1}\widetilde{M}^\top + \Sigma(R_{\mathrm{g}}\Lambda_{\mathrm{g}})^{-1}\Big)^{-1}. \tag{34n}$$

D. Model-order Reduction via Singular Perturbation

Upon setting $\epsilon = 0$ in (34), the differential equations associated with fast-varying state variables are transformed to algebraic expressions. These can then be used to eliminate all fast-varying states from the resulting system of equations, thereby reducing the model-order.

1) Solving for e_k', $p_{\mathrm{m},k}$, and $q_{\mathrm{m},k}$: Setting $\epsilon = 0$ in (34k)–(34m), and solving for e_k', $p_{\mathrm{m},k}$, and $q_{\mathrm{m},k}$, we have that

$$e_k' = \frac{1}{c_k}\mathrm{T}(\tfrac{\pi}{2})\big(i_{\mathrm{i},k}' - i_{\mathrm{g},k}'\big). \tag{35a}$$

$$p_{\mathrm{m},k} = {e_k'}^\top i_{\mathrm{g},k}', \tag{35b}$$

$$q_{\mathrm{m},k} = {e_k'}^\top \mathrm{T}(-\tfrac{\pi}{2})i_{\mathrm{g},k}'. \tag{35c}$$

2) Solving for γ_k'': Setting $\epsilon = 0$ in (34j) and solving for $i_{\mathrm{i},k}'$, we have that

$$i_{\mathrm{i},k}' = \rho_k\frac{k_{\mathrm{Pi},k}}{r_{\mathrm{i},k} + k_{\mathrm{Pi},k}}\big(k_{\mathrm{Pv},k}(\mathrm{T}(-\delta_k)\mathbb{e}_1 E_k^\circ - e_k') + i_{\mathrm{g},k}' - \mathrm{T}(\tfrac{\pi}{2})c_k e_k' + k_{\mathrm{Iv},k}\mathrm{T}(-\delta_k)\phi_k''\big) + \frac{k_{\mathrm{Ii},k}}{r_{\mathrm{i},k} + k_{\mathrm{Pi},k}}\mathrm{T}(-\delta_k)\gamma_k''. \tag{36a}$$

Substituting (36a) into (34h), and setting $\epsilon = 0$, we have

$$\frac{r_{\mathrm{i},k} + k_{\mathrm{Pi},k}}{\omega_0 k_{\mathrm{Ii},k}}\frac{\mathrm{d}\gamma_k''}{\mathrm{d}t} = -\gamma_k'' + \frac{\rho_k r_{\mathrm{i},k}}{k_{\mathrm{Ii},k}}\big(k_{\mathrm{Pv},k}(\mathbb{e}_1 E_k^\circ - \mathrm{T}(\delta_k)e_k') + k_{\mathrm{Iv},k}\phi_k'' - c_k \mathrm{T}(\delta_k + \tfrac{\pi}{2})e_k' + \mathrm{T}(\delta_k)i_{\mathrm{g},k}'\big). \tag{36b}$$

From Assumption 3, $\frac{r_{\mathrm{i},k} + k_{\mathrm{Pi},k}}{\omega_0 k_{\mathrm{Ii},k}} = \lambda_7\epsilon$. Substituting this into (36b), and setting $\epsilon = 0$, we have

$$\gamma_k'' = \frac{r_{\mathrm{i},k}}{k_{\mathrm{Ii},k}}\rho_k\big(k_{\mathrm{Pv},k}(\mathbb{e}_1 E_k^\circ - \mathrm{T}(\delta_k)e_k') + k_{\mathrm{Iv},k}\phi_k'' - c_k \mathrm{T}(\delta_k + \tfrac{\pi}{2})e_k' + \mathrm{T}(\delta_k)i_{\mathrm{g},k}'\big). \tag{36c}$$

3) Solving for ϕ_k'' and $i_{\mathrm{i},k}'$: Substituting (36c) into (36a) gives the expressions

$$i_{\mathrm{i},k}' = \rho_k\Big(k_{\mathrm{Pv},k}(\mathrm{T}(-\delta_k)\mathbb{e}_1 E_k^\circ - e_k') + i_{\mathrm{g},k}' - \mathrm{T}(\tfrac{\pi}{2})c_k e_k' + k_{\mathrm{Iv},k}\mathrm{T}(-\delta_k)\phi_k''\Big), \tag{37a}$$

from where it follows that

$$\mathbb{e}_1 E_k^\circ - \mathrm{T}(\delta_k)e_k' = \frac{1}{\rho_k k_{\mathrm{Pv},k}}\mathrm{T}(\delta_k)i_{\mathrm{i},k}' - \frac{1}{k_{\mathrm{Pv},k}}\mathrm{T}(\delta_k)i_{\mathrm{g},k}' + \mathrm{T}(\delta_k + \tfrac{\pi}{2})\frac{c_k}{k_{\mathrm{Pv},k}}e_k' - \frac{k_{\mathrm{Iv},k}}{k_{\mathrm{Pv},k}}\phi_k''. \tag{37b}$$

Substituting (37b) into (34g) and setting $\epsilon = 0$ results in the expression

$$\frac{k_{\mathrm{Pv},k}}{\omega_0}\frac{\mathrm{d}\phi_k''}{\mathrm{d}t} = \frac{\rho_k - 1}{\rho_k}k_{\mathrm{a},k}k_{\mathrm{Pv},k}\mathrm{T}(\delta_k)i_{\mathrm{i},k}' + \frac{1}{\rho_k}\mathrm{T}(\delta_k)i_{\mathrm{i},k}'$$

$$- \mathrm{T}(\delta_k) i'_{\mathrm{g},k} + \mathrm{T}(\delta_k + \tfrac{\pi}{2}) c_k e'_k - k_{\mathrm{Iv},k} \phi''_k. \quad (37c)$$

Substituting (35a) into (37c), while leveraging the fact that $\mathrm{T}(\delta_k + \frac{\pi}{2})\mathrm{T}(\frac{\pi}{2}) = -\mathrm{T}(\delta_k)$, gives

$$\frac{k_{\mathrm{Pv},k}}{\omega_0 k_{\mathrm{Iv},k}} \frac{\mathrm{d}\phi''_k}{\mathrm{d}t} = -\phi''_k + \frac{\rho_k - 1}{\rho_k} \frac{k_{\mathrm{a},k} k_{\mathrm{Pv},k} - 1}{k_{\mathrm{Iv},k}} \mathrm{T}(\delta_k) i'_{\mathrm{i},k}. \quad (37d)$$

From Assumption 3, $\frac{k_{\mathrm{Pv},k}}{\omega_0 k_{\mathrm{Iv},k}} = \lambda_7 \epsilon$. Substituting this into (37d), and setting $\epsilon = 0$, we have

$$\phi''_k = \frac{\rho_k - 1}{\rho_k} \frac{k_{\mathrm{a},k} k_{\mathrm{Pv},k} - 1}{k_{\mathrm{Iv},k}} \mathrm{T}(\delta_k) i'_{\mathrm{i},k}. \quad (37e)$$

Substituting (35a) and (37e) into (37a) and solving for $i'_{\mathrm{i},k}$, we have that

$$i'_{\mathrm{i},k} = \rho_k (\mathrm{A}_{1,k}(\rho) i'_{\mathrm{g},k} + \mathrm{A}_{1,k}(\rho) \mathbb{e}_1 E^\circ_k), \quad (37f)$$

with matrices $\mathrm{A}_{1,k}(\rho)$ and $\mathrm{A}_{2,k}(\rho)$ defined in (29).

4) Solving for η_k and α_k: Let $\widetilde{\omega}_k$ denote the bus voltage frequency at bus k. Then, (34f) can be rewritten as

$$\frac{1}{\omega_0 k_{\mathrm{P}\theta,k}} \frac{\mathrm{d}\alpha_k}{\mathrm{d}t} = \mathbb{e}_2^\top \mathrm{T}(\alpha_k + \delta_k) v'_k + \frac{k_{\mathrm{I}\theta,k}}{k_{\mathrm{P}\theta,k}} \eta_k. \quad (38a)$$

From Assumption 3, $\frac{1}{\omega_0 k_{\mathrm{P}\theta,k}} = \lambda_5 \epsilon$. Substituting this into (38a), and setting $\epsilon = 0$, we have

$$\mathbb{e}_2^\top \mathrm{T}(\alpha_k + \delta_k) v'_k = -\frac{k_{\mathrm{I}\theta,k}}{k_{\mathrm{P}\theta,k}} \eta_k. \quad (38b)$$

Substituting (38b) into (34e) gives

$$\frac{k_{\mathrm{P}\theta,k}}{\omega_0 k_{\mathrm{I}\theta,k}} \frac{\mathrm{d}\eta_k}{\mathrm{d}t} = -\eta_k. \quad (38c)$$

Using steady-state initial conditions for the reduced-order model, (38b) and (38c) result in

$$\eta_k = 0, \qquad \alpha_k = \arctan\left(\frac{\mathbb{e}_2^\top v'_k}{\mathbb{e}_1^\top v'_k}\right) - \delta_k. \quad (38d)$$

E. Reduced-order Model

Combining results in Appendices C and D gives the following reduced-order model

$$\frac{\mathrm{d}\delta_k}{\mathrm{d}t} = \omega^\circ_k - \omega_0, \quad (39a)$$

$$\frac{\mathrm{d}\omega^\circ_k}{\mathrm{d}t} = \frac{1}{f_{\mathrm{f},k}(E^\circ_k)} \frac{1}{\tau_{\mathrm{f},k}} \mathbb{e}_1^\top \mathrm{T}(\psi_k - \tfrac{\pi}{2}) \begin{bmatrix} p^\star_k - p_{\mathrm{m},k} \\ q^\star_k - q_{\mathrm{m},k} \end{bmatrix} + \frac{1}{\tau_{\mathrm{f},k}} (\omega_0 - \omega^\circ_k), \quad (39b)$$

$$\frac{\mathrm{d}E^\circ_k}{\mathrm{d}t} = \frac{1}{f_{\mathrm{v},k}(E^\circ_k)} \frac{1}{\tau_{\mathrm{v},k}} \mathbb{e}_2^\top \mathrm{T}(\psi_k - \tfrac{\pi}{2}) \begin{bmatrix} p^\star_k - p_{\mathrm{m},k} \\ q^\star_k - q_{\mathrm{m},k} \end{bmatrix} + \frac{1}{\tau_{\mathrm{v},k}} f_{\mathrm{e},k}(E^\star_k, E^\circ_k), \quad (39c)$$

$$\frac{\mathrm{d}i'_{\mathrm{g},k}}{\mathrm{d}t} = \Big(\omega_0 \mathrm{T}(\tfrac{\pi}{2}) - \frac{\omega_0 r_{\mathrm{g},k}}{l_{\mathrm{g},k}} \mathbb{I}\Big) i'_{\mathrm{g},k} + \frac{\omega_0}{l_{\mathrm{g},k}} (e'_k - v'_k), \quad (39d)$$

$$0 = \rho_k + \varepsilon \ln\left(\exp\left(-\frac{1}{\varepsilon}\right) + \exp\left(-\frac{i_{\max}\sqrt{c_k^2 k_{\mathrm{a},k}^2 (\rho_k - 1)^2 + {\rho_k}^2}}{\varepsilon \| c_k \mathbb{e}_2 E^\circ_k + \mathrm{T}(\delta_k) i'_{\mathrm{g},k} \|_2}\right)\right), \quad (39e)$$

$$v'_{\mathcal{I}} = \Big(i'_{\mathcal{I}}\Big(\frac{1}{\tau_{\mathrm{t}}} \mathbb{I} - \Lambda_{\mathrm{g}}^{-1}\Big) + e'_{\mathcal{I}} (R_{\mathrm{g}} \Lambda_{\mathrm{g}})^{-1}\Big)\Big(\frac{1}{\tau_{\mathrm{t}}} \widetilde{M} \widetilde{R}^{-1} \widetilde{M}^\top + \Sigma (R_{\mathrm{g}} \Lambda_{\mathrm{g}})^{-1}\Big)^{-1}. \quad (39f)$$

The evolution of the fast varying state variables can be described by the following algebraic expressions

$$p_{\mathrm{m},k} = {e'_k}^\top i'_{\mathrm{g},k}, \quad (40a)$$

$$q_{\mathrm{m},k} = {e'_k}^\top \mathrm{T}(-\tfrac{\pi}{2}) i'_{\mathrm{g},k}, \quad (40b)$$

$$\eta_k = 0, \quad (40c)$$

$$\alpha_k = \arctan\left(\frac{\mathbb{e}_2^\top v'_k}{\mathbb{e}_1^\top v'_k}\right) - \delta_k, \quad (40d)$$

$$i'_{\mathrm{i},k} = \rho_k (\mathrm{A}_{1,k}(\rho) i'_{\mathrm{g},k} + \mathrm{A}_{1,k}(\rho) \mathbb{e}_1 E^\circ_k), \quad (40e)$$

$$e'_k = \frac{1}{c_k} \mathrm{T}(\tfrac{\pi}{2}) \big(i'_{\mathrm{i},k} - i'_{\mathrm{g},k}\big), \quad (40f)$$

$$\phi''_k = \frac{\rho_k - 1}{\rho_k} \frac{k_{\mathrm{a},k} k_{\mathrm{Pv},k} - 1}{k_{\mathrm{Iv},k}} \mathrm{T}(\delta_k) i'_{\mathrm{i},k}, \quad (40g)$$

$$\gamma''_k = \frac{r_{\mathrm{i},k}}{k_{\mathrm{Ii},k}} \mathrm{T}(\delta_k) i'_{\mathrm{i},k}. \quad (40h)$$

ACKNOWLEDGEMENT

Assistance from D. Venkatramanan on key graphics is appreciated.

REFERENCES

[1] Y. Lin, J. H. Eto, B. B. Johnson, J. D. Flicker, R. H. Lasseter, H. N. V. Pico, G.-S. Seo, B. J. Pierre, and A. Ellis, "Research roadmap on grid-forming inverters," Tech. Rep., National Renewable Energy Laboratory, NREL/TP-5D00-73476, 2020.

[2] J. Rocabert, A. Luna, F. Blaabjerg, and P. Rodríguez, "Control of power converters in AC microgrids," *IEEE Transactions on Power Electronics*, vol. 27, no. 11, pp. 4734–4749, 2012.

[3] M. C. Chandorkar, D. M. Divan, and R. Adapa, "Control of parallel connected inverters in standalone AC supply systems," *IEEE Trans. Ind. Appl.*, vol. 29, no. 1, pp. 136–143, Jan. 1993.

[4] N. Pogaku, M. Prodanovic, and T. C. Green, "Modeling, analysis and testing of autonomous operation of an inverter-based microgrid," *IEEE Trans. Power Electron.*, vol. 22, no. 2, pp. 613–625, Mar. 2007.

[5] Q.-C. Zhong and G. Weiss, "Synchronverters: Inverters that mimic synchronous generators," *IEEE Trans. Ind. Electron.*, vol. 58, no. 4, pp. 1259–1267, Apr. 2011.

[6] S. D'Arco, J. Suul, and O. Fosso, "A virtual synchronous machine implementation for distributed control of power converters in smartgrids," *Electric Power Systems Research*, vol. 122, pp. 180 – 197, 2015.

[7] J. Liu, Y. Miura, H. Bevrani, and T. Ise, "Enhanced virtual synchronous generator control for parallel inverters in microgrids," *IEEE Trans. Smart Grid*, vol. 8, no. 5, pp. 2268–2277, Sep. 2017.

[8] L. A. Tôrres, J. P. Hespanha, and J. Moehlis, "Synchronization of Identical Oscillators Coupled Through a Symmetric Network With Dynamics: A Constructive Approach With Applications to Parallel Operation of Inverters," *IEEE Trans. Autom. Control*, vol. 60, no. 12, pp. 3226–3241, Dec. 2015.

[9] M. Li, Y. Gui, Y. Guan, J. Matas, J. M. Guerrero, and J. C. Vasquez, "Inverter parallelization for an islanded microgrid using the Hopf oscillator controller approach with self-synchronization capabilities," *IEEE Trans. Ind. Electron.*, pp. 1–1, 2020.

[10] M. Colombino, D. Groß, J. Brouillon, and F. Dörfler, "Global phase and magnitude synchronization of coupled oscillators with application to the control of grid-forming power inverters," *IEEE Trans. Autom. Control*, vol. 64, no. 11, pp. 4496–4511, Nov. 2019.

[11] A. Tayyebi, D. Groß, A. Anta, F. Kupzog, and F. Dörfler, "Frequency stability of synchronous machines and grid-forming power converters," *IEEE Journal of Emerging and Selected Topics in Power Electronics*, vol. 8, no. 2, pp. 1004–1018, 2020.

[12] O. Ajala, M. Lu, S. Dhople, B. B. Johnson, and A. Domínguez-García, "Model reduction for inverters with current limiting and dispatchable virtual oscillator control," *IEEE Trans. Energy Convers.*, 2021.

[13] M. G. Taul, X. Wang, P. Davari, and F. Blaabjerg, "Current limiting control with enhanced dynamics of grid-forming converters during fault conditions," *IEEE Journal of Emerging and Selected Topics in Power Electronics*, vol. 8, no. 2, pp. 1062–1073, 2020.

[14] A. J. Germond and R. Podmore, "Dynamic aggregation of generating unit models," *IEEE Trans. Power Apparatus and Systems*, vol. PAS-97, no. 4, pp. 1060–1069, July 1978.

[15] I. J. Perez-Arriaga, G. C. Verghese, and F. C. Schweppe, "Selective modal analysis with applications to electric power systems, Part I: heuristic introduction," *IEEE Power Engineering Review*, vol. PER-2, no. 9, pp. 29–30, Sept. 1982.

[16] G. N. Ramaswamy, L. Rouco, O. Fillatre, G. C. Verghese, P. Panciatici, B. C. Lesieutre, and D. Peltier, "Synchronic modal equivalencing (SME) for structure-preserving dynamic equivalents," *IEEE Trans. Power Syst.*, vol. 11, no. 1, pp. 19–29, Feb. 1996.

[17] G. Kron, "A method of solving very large physical systems in easy stages," *Proc. of the IRE*, vol. 42, no. 4, pp. 680–686, 1954.

[18] P. Kokotovic, J. Allemong, W. James, and C. Joe, "Singular perturbation and iterative separation of time scales," *Automatica*, vol. 16, no. 1, pp. 23–33, 1980.

[19] K. Kodra, N. Zhong, and Z. Gajić, "Model order reduction of an islanded microgrid using singular perturbations," in *Proc. of the American Control Conference*, Aug. 2016, pp. 3650–3655.

[20] F. Dörfler and F. Bullo, "Synchronization and transient stability in power networks and nonuniform Kuramoto oscillators," *SIAM Journal on Control and Optimization*, vol. 50, no. 3, pp. 1616–1642, 2012.

[21] J. Schiffer, D. Zonetti, R. Ortega, A. M. Stankovic, T. Sezi, and J. Raisch, "A survey on modeling of microgrids—from fundamental physics to phasors and voltage sources," *Automatica*, vol. 74, May 2015.

[22] L. Luo and S. V. Dhople, "Spatiotemporal model reduction of inverter-based islanded microgrids," *IEEE Trans. Energy Convers.*, vol. 29, no. 4, pp. 823–832, Dec. 2014.

[23] M. Rasheduzzaman, J. A. Mueller, and J. W. Kimball, "Reduced-order small-signal model of microgrid systems," *IEEE Trans. Sustain. Energy*, vol. 6, no. 4, pp. 1292–1305, 2015.

[24] O. Ajala, A. Domínguez-García, and P. Sauer, *A Hierarchy of Models for Inverter-Based Microgrids*. Springer-Verlag, Berlin, 2017.

[25] P. Vorobev, P. Huang, M. A. Hosani, J. Kirtley, and K. Turitsyn, "High-fidelity model order reduction for microgrids stability assessment," *IEEE Trans. Power Syst.*, vol. 33, no. 1, pp. 874–887, Jan 2018.

[26] M. Lu, S. Dutta, V. Purba, S. Dhople, and B. Johnson, "A grid-compatible virtual oscillator controller: Analysis and design," in *IEEE Energy Conversion Congress and Exposition*, 2019, pp. 2643–2649.

[27] I. Caduff, U. Markovic, C. Roberts, G. Hug, and E. Vrettos, "Reduced-order modeling of inverter-based generation using hybrid singular perturbation," *Electric Power Systems Research*, vol. 190, p. 106773, 2021.

[28] S. Y. Caliskan and P. Tabuada, "Kron reduction of power networks with lossy and dynamic transmission lines," in *Proc. of the IEEE Conference on Decision and Control (CDC)*, 2012, pp. 5554–5559.

[29] A. Yazdani and R. Iravani, *Voltage-Sourced Converters in Power Systems*. Wiley, Jan. 2010.

[30] O. Ajala, N. Baeckeland, S. Dhople, and A. Domínguez-García, "Uncovering the Kuramoto Model from Full-order Models of Grid-forming Inverter-based Power Networks," in *Proc. of the IEEE Conference on Decision and Control (CDC)*, Dec 2021.

[31] P. Kundur, N. J. Balu, and M. G. Lauby, *Power System Stability and Control*. McGraw-Hill, 1994.

[32] P. Kokotović, H. K. Khalil, and J. O'Reilly, *Singular Perturbation Methods in Control: Analysis and Design*, ser. Classics in Applied Mathematics. Society for Industrial and Applied Mathematics, 1986.

[33] B. Johnson, T. Roberts, O. Ajala, A. Domínguez-García, S. Dhople, D. Ramasubramanian, A. Tuohy, D. Divan, and B. Kroposki, "A generic primary-control model for grid-forming inverters: Towards interoperable operation & control," in *Proc. of the 55th Hawaii International Conference on System Sciences (HICSS), Maui, HI, USA*, 2022.

[34] M. M. S. Khan, Y. Lin, B. Johnson, V. Purba, M. Sinha, and S. Dhople, "A reduced-order aggregated model for parallel inverter systems with virtual oscillator control," in *IEEE Workshop on Control and Modeling for Power Electronics*, 2018, pp. 1–6.

[35] R. A. Horn and C. R. Johnson, *Norms for vectors and matrices*. Cambridge University Press, 1985, p. 257–342.

[36] M. K. Singh, S. Dhople, F. Dörfler, and G. B. Giannakis, "Time-domain generalization of kron reduction," *IEEE Control Systems Letters*, vol. 7, pp. 259–264, 2023.

[37] (1993) 14 bus power flow test case. [Online]. Available: http://labs.ece.uw.edu/pstca/pf14/pg_tca14bus.htm

[38] (1993) 118 bus power flow test case. [Online]. Available: http://labs.ece.uw.edu/pstca/pf118/pg_tca118bus.htm

Olaoluwapo (Olaolu) Ajala (Member, IEEE) received the B.Sc. degree in Electrical and Electronics Engineering from the University of Lagos in 2010, and the M.Sc. and Ph.D. degrees in Electrical and Computer Engineering from the University of Illinois at Urbana-Champaign in 2014 and 2018 respectively. He is a Research Engineer in the Department of Electrical and Computer Engineering at the University of Illinois at Urbana-Champaign, where he is affiliated with the Power and Energy Systems area. His research interests include microgrids modeling, analysis and control, and hardware implementation of microgrid control architectures.

Nathan Baeckeland (Student Member, IEEE) received the B.S., M.S., and Ph.D. degrees in Electrical Engineering from the KU Leuven, Belgium, in 2017, 2018 and 2022, respectively. From 2020 to 2021, he was affiliated with the University of Minnesota,Minneapolis, MN, USA, as a doctoral fellow of the Belgian American Education Foundation (BAEF). His current research focus lies on the design and modeling of inverter control systems for fault studies and power system protection analysis.

Brian Johnson (Member, IEEE) obtained his M.S. and Ph.D. degrees in Electrical and Computer Engineering from the University of Illinois at Urbana-Champaign, Urbana, in 2010 and 2013, respectively. He is currently an Assistant Professor in the Department of Electrical and Computer Engineering at The University of Texas at Austin. Previously, he was with the Department of Electrical and Computer Engineering at the University of Washington in Seattle and also spent several of his earlier years at the National Renewable Energy Laboratory in Colorado. His work was recognized with a National Science Foundation (NSF) CAREER Award in 2022. He is currently co-leading the multi-institutional Universal Interoperability for Grid-Forming Inverters (UNIFI) Consortium which is funded by the U.S. Department of Energy (DOE). His research interests are in renewable energy systems, power electronics, and control systems.

Sairaj V. Dhople (Senior Member, IEEE) received the B.S., M.S., and Ph.D. degrees in electrical engineering from the University of Illinois at Urbana-Champaign, Urbana, IL, USA, in 2007, 2009, and 2012, respectively. He is currently Robert & Sydney Anderson Associate Professor with the Department of Electrical and Computer Engineering, University of Minnesota, Minneapolis, MN, USA. His research interests include modeling, analysis, and control of power electronics and power systems with a focus on renewable integration. Dr. Dhople is the recipient of the National Science Foundation CAREER Award in 2015, the Outstanding Young Engineer Award from the IEEE Power and Energy society in 2019, and the IEEE Power and Energy Society Prize Paper Award in 2021.

Alejandro D. Domínguez-García (Fellow, IEEE) received the the master's degree in electrical engineering from the University of Oviedo (Spain) in 2001 and the Ph.D. degree in electrical engineering and computer science from the Massachusetts Institute of Technology, Cambridge, MA, in 2007.

He is Professor with the Department of Electrical and Computer Engineering (ECE), and Research Professor with the Coordinated Science Laboratory and the Information Trust Institute, all at the University of Illinois at Urbana-Champaign. He is affiliated with the ECE Power and Energy Systems area, and has been a Grainger Associate since 2011, and a William L. Everitt Scholar since 2017.

His research program aims at the development of technologies for providing a reliable and efficient supply of electricity—a key to ensuring societal welfare and sustainable economic growth. Specific activities within his program include work on: (i) control of distributed energy resources, (ii) power system health monitoring and reliability analysis, and (iii) quantifying and mitigating the impact of renewable-based generation

Dr. Domínguez-García received the NSF CAREER Award in 2010, and the Young Engineer Award from the IEEE Power and Energy Society in 2012. In 2014, he was invited by the National Academy of Engineering to attend the US Frontiers of Engineering Symposium, and was selected by the University of Illinois at Urbana-Champaign Provost to receive a Distinguished Promotion Award. In 2015, he received the U of I College of Engineering Dean's Award for Excellence in Research. In 2023, he was elevated to IEEE Fellow for contributions to distributed control and uncertainty analysis of electrical energy systems.

He is currently an associate editor of the IEEE Transactions on Power Systems and the IEEE Power Engineering Letters. He also served as an editor of the IEEE Transactions on Control of Network Systems from July 2018 to June 2021.